NUMERICAL SIMULATION OF SINGLE AND DOUBLE SLOPE SOLAR STILL FOR DIFFERENT VARIABLES

A DISSERTATION

SUBMITTED IN PARTIAL FULFILLMENT OF THE REQUIREMENTS FOR THE AWARD OF THE DEGREE

OF

MASTER OF TECHNOLOGY

IN

THERMAL ENGINEERING

Submitted by

ROHIT KUMAR

(2K18/THE/23)

Under the supervision of

DR. ANIL KUMAR

DEPARTMENT OF MECHANICAL ENGINEERING
DELHI TECHNOLOGICAL UNIVERSITY
(Formerly Delhi College of Engineering)
Bawana Road, Delhi- 110042 (India)

AUGUST 2020

DELHI TECHNOLOGICAL UNIVERSITY
(Formerly Delhi College of Engineering)
Bawana Road, Delhi- 110042 (India)

CANDIDATE'S DECLARATION

I, ROHIT KUMAR, Roll No. 2K18/THE/23 student of M.Tech (Thermal Engineering), hereby declare that the project dissertation titled "**Numerical Simulation of Single and Double Slope Solar Stills for Different Variables**" which is submitted by me to the Department of Mechanical Engineering, Delhi Technological University, Delhi (India) in partial fulfillment of the requirement for the award of the degree of Master of Technology is original and not copied from any source without proper citation. This work has not previously formed the basis for the award of any Degree, Diploma Associateship Fellowship, or other similar title or recognition.

Place: Delhi
Date: 26 AUGUST 2020

ROHIT KUMAR
(2K18/THE/23)

DEPARTMENT OF MECHANICAL ENGINEERING
DELHI TECHNOLOGICAL UNIVERSITY
(Formerly Delhi College of Engineering)
Bawana Road, Delhi- 110042 (India)

CERTIFICATE

I hereby certify that the Project Dissertation titled "**NUMERICAL SIMULATION OF SINGLE AND DOUBLE SLOPE SOLAR STILLS FOR DIFFERENT VARIABLES**" which is submitted by **ROHIT KUMAR**, Roll No. **2K18/THE/23** Department 0f Mechanical Engineering, Delhi Technological University, Delhi in partial fulfillment of the requirement for the award of the degree of Master of Technology, is a record of the project work carried out by the student under my supervision. To the best of my knowledge, this work has not been submitted in part or full for any Degree or Diploma to this University or elsewhere.

Place: Delhi
Date: 26 AUGUST 2020

Dr. ANIL KUMAR
SUPERVISOR
(Associate Professor)
Delhi Technological University
(Formerly Delhi College of Engineering)
Bawana Road, Delhi -110042

Abstract

Water and the use of conventional energy sources are two significant problems in the world. Water is essential for sustenance. Human beings need of potable water at less consumption of non- renewable energy resources. There are many techniques to convert saline water into potable water. In this paper, three-phase, three dimensional a single slope and double slope single basin still both were prepared and simulated by using ANSYS FLUENT v19.2. Simulation results of solar stills were made by using evaporation as well as condensation process at the climate conditions of Delhi (27.0238° N, 74.2179° E). Within the scope of this study, simulation results of both systems were calculated and compared with each other. It is examined that the temperature inside the single slope solar still is maximum from 13:00 to 14:00 hrs while the double slope still has low temperature compared to the single still. The maximum and minimum temperature of the water-vapor mixture inside the single slope still were calculated 435.39K and 22.283K and the maximum and minimum temperature on glass were 379 K and 16.22 K whereas in double slope, the maximum and minimum temperature of the water-vapor mixture inside the still were 92.12K and 25.60K and glass temperature were 76.154K and 19.22K. Hence, due to the temperature difference between the glass surface and outer environment, more condensation will be in the single slope solar still. Inner water temperature is responsible for more evaporation and higher temperature more than 50°C can be found in single slope solar still as compared to the double slope. The maximum water production rate in single slope solar still is 0.84 kg $m^{-2}hr^{-1}$ while the maximum water production rate in the double slope is 0.26 kg $m^{-2}hr^{-1}$. In the simulation, all other variables are also checked and calculated, also observed single slope solar still has a high value of all variables which affect water production. Hence, the single slope solar still could be better there.

Keywords: Solar Still, Computational Fluid Dynamics Analysis, Water temperature, Water Productivity

DEPARTMENT OF MECHANICAL ENGINEERING
DELHI TECHNOLOGICAL UNIVERSITY
(Formerly Delhi College of Engineering)
Bawana Road, Delhi- 110042

ACKNOWLEDGEMENT

First of all, I thank almighty God for his blessings, who gave me the opportunity and strength to carry out this work. I want to express my profound sense of deepest gratitude and sincere thanks to my honorable and esteemed guide DR. ANIL KUMAR, Associate Professor, Department of Mechanical Engineering, Delhi Technological University, Delhi (India) for his exemplary guidance, monitoring, and consent encouragement and untiring support. The blessings, help, and guidance given by him time to time shall carry me a long way in the journey of life on which I am about to embark. I am glad to have worked with him. He has been a great source of inspiration to me, and I thank him from the bottom of my heart.

ROHIT KUMAR
(2K18/THE/23)

CONTENTS

Candidate's Declaration i

Certificate ii

Acknowledgement iii

Abstract iv

Contents

List of Tables 4

List of Figures 5

List of Symbols, abbreviations 7

CHAPTER 1 INTRODUCTION 8

1.1 Membrane desalination process 12

1.1.1 Reverse Osmosis 13

1.1.2 Electrodialysis 13

1.2. Thermal desalination process 13

1.2.1 Multi-Effect distillation (MED) 13

1.2.2 Multi-Stage Flash (MSF) 14

1.2.3 Solar Stills 15

CHAPTER 2 LITERATURE REVIEW 17

CHAPTER 3 METHODOLOGY 26

3.1 Governing Equations 26

3.1.1 Energy Equation 27

3.1.2 Continuity Equation 27

3.1.3 Momentum Equation 27

3.1.4 Volume conservation equation 28

3.1.5 Mass transfer equation 29

3.1.6 Pressure Constraint 29

3.1.7 Heat transfer equation 30

3.1.8 Water production 30

3.1.9 Solar irradiance equation 31

3.2 Computational Fluid Dynamics Model of Modeling 28

3.2.1 Geometry Creation 28

3.2.2 Meshing 30

3.2.3 Boundary Conditions and initial conditions 31

CHAPTER 4 RESULT AND DISCUSSION 33

4.1 Simulation Results 33

4.1.1 Temperature Distribution 33

4.1.2 Temperature Distribution with Time 35

4.1.3 Water Volume Fraction 36

4.1.4 Pressure Variation 45

4.1.5 Velocity Distribution 49

4.1.6 Mass Flow 50

4.1.7 Static Enthaply 52

4.1.8 Absorption Coefficient 55

4.1.9 Do Irradiation 57

4.1.10 Eddy Viscosity 58

4.1.11 Solar Heat Flux 60

4.1.12 Water Production Rate 62

CHAPTER 5 CONCLUSION 65

REFERENCES 67

LIST OF TABLES

Table 1	Effect of fluoride level in potable water on human beings
Table 2	Boundary conditions for the simulation process of single slope and double slope.

LIST OF FIGURES

Figure 1 World water distribution on the earth
Figure 2 Reported cases and death by water-borne diseases in India
Figure 3 The occurrence of fluoride in groundwater of Asia
Figure 4 Different desalination process chart
Figure 5 Schematic diagram of multi-stage flash
Figure 6 Annual average normal solar irradiance for various states of India
Figure 7 Solar irradiance concerning months
Figure 8 The single slope solar basin
Figure 9 Double slope solar basin
Figure 10 a. Single Slope Single Solar Still
b. Double Slope Single Solar Still
Figure 11 a. The unstructured mesh of single slope
b. The unstructured mesh of double slope still.
Figure 12 a. Temperature distribution inside the single slope solar basin
b. Temperature distribution inside the double slope solar still
Figure 13 Temperature variation concerning the time of single slope solar still
Figure 14 Temperature variation concerning the time of double slope solar still
Figure 15 Water volume fraction contour inside the glass of single slope still.
Figure 16 Water volume fraction contour on the glass of single slope still.
Figure 17 Water volume fraction contour on the glass of double slope still
Figure 18 Water volume fraction contour inside the glass of double slope still.
Figure 19 a. Vapor volume fraction contour inside the single slope solar still.
b. Vapor volume fraction contour on the glass of single slope solar still.
Figure 20 a. Vapor volume fraction contour on the glass of double slope solar still
b. Vapor volume fraction contour inside the double slope solar still
Figure 21 Water volume fraction concerning the time of single slope solar still.
Figure 22 Vapor volume fraction concerning the time of single slope solar still.
Figure 23 Vapor volume fraction concerning the time of double slope solar still
Figure 24 Pressure volume rendering inside the single slope solar still
Figure 25 Pressure volume rendering inside the double slope solar still.
Figure 26 Pressure variation concerning time inside single slope solar still
Figure 27 Pressure variation concerning time inside double slope solar still.
Figure 28 Velocity volume rendering inside the single slope solar still

Figure 29 Velocity volume rendering inside the double slope solar still
Figure 30 Mass flow contour inside the double slope solar still
Figure 31 Mass flow contour inside the double slope solar still
Figure 32 Static enthalpy volume rendering inside the double slope solar still
Figure 33 Static enthalpy volume rendering inside the double slope solar still.
Figure 34 Absorption coefficient volume rendering inside the single slope solar still.
Figure 35 Absorption coefficient volume rendering inside the double slope solar still.
Figure 36 a. Do irradiation volume rendering inside the single slope solar still.
b. Do irradiance volume rendering inside the double slope solar still.
Figure 37 Eddy viscosity volume rendering inside the single slope solar still.
Figure 38 Eddy viscosity volume rendering inside the double slope solar still.
Figure 39 Solar heat flux concerning time inside the single slope solar still.
Figure 40 Solar heat flux concerning time inside the double slope solar still.
Figure 41 Water production rate concerning time inside the single slope solar still.
Figure 42 Water production rate concerning time inside the double slope solar still.

LIST OF SYMBOLS

$\overline{v_m}$ = the mass averaged velocity

k_t = the turbulent thermal conductivity which is defined according to the turbulence model

a_k = the absorptivity

S_E = sum of the heat of chemical reaction, and any other volumetric heat sources

ρ_m = Density of mixture

$\bar{F}$ = The gravitational body force and external body forces

μ_m= molecular viscosity of the mixture

r_G = volume fraction of gas.

r_L = volume fraction of liquid.

$h_p^{f^i}$= formation enthalpy of species i of phase p.

$h_q^{f^j}$ = formation enthalpy of species i of phase q.

h_p^i = enthalpy of species i of phase p.

H_p = total enthalpy of phase p

Hq = total enthalpy of phase q.

$h_{r\omega}$ = radiative heat transfer coefficient form water to the glass, W/m^2°C

h_{cw} = convective heat transfer coefficient from water to the glass, W/m^2°C.

$h_{e\omega}$ = evaporative heat transfer coefficient from water to the glass, W/m^2°C.

ε_ω = emissivity

T_w = temperature of the water.

P_w = Partial saturated vapor pressure at the water temperature.

Pg = Partial saturated vapor pressure at the gas temperature

σ = Stephan Boltzman, W/m^2 °C

$\dot{m}_{ew}$= distillate output

h_{fg} = Latent heat of vaporization of water, J/Kg.

δ = sun declination angle

n = day of the year, starting from 1st January

ω = Hour angle, degree.

Ig = Hourly global irradiance

I_b = Hourly diffuse radiation

I_d = Hourly diffuse radiation

I_{bn} = Beam radiation on the surface normal to the direction of the sun rays.

DSSS = Double slope solar still

TDS = Total dissolved solids

SSS = Single slope solar still

RE = Renewable energy

SE = Solar Energy

D = Desalination

CHAPTER 1

INTRODUCTION

Freshwater is a key resource and it is a basic need to survive for humans life. But, there is a limitation of freshwater supply on the surface of the earth.

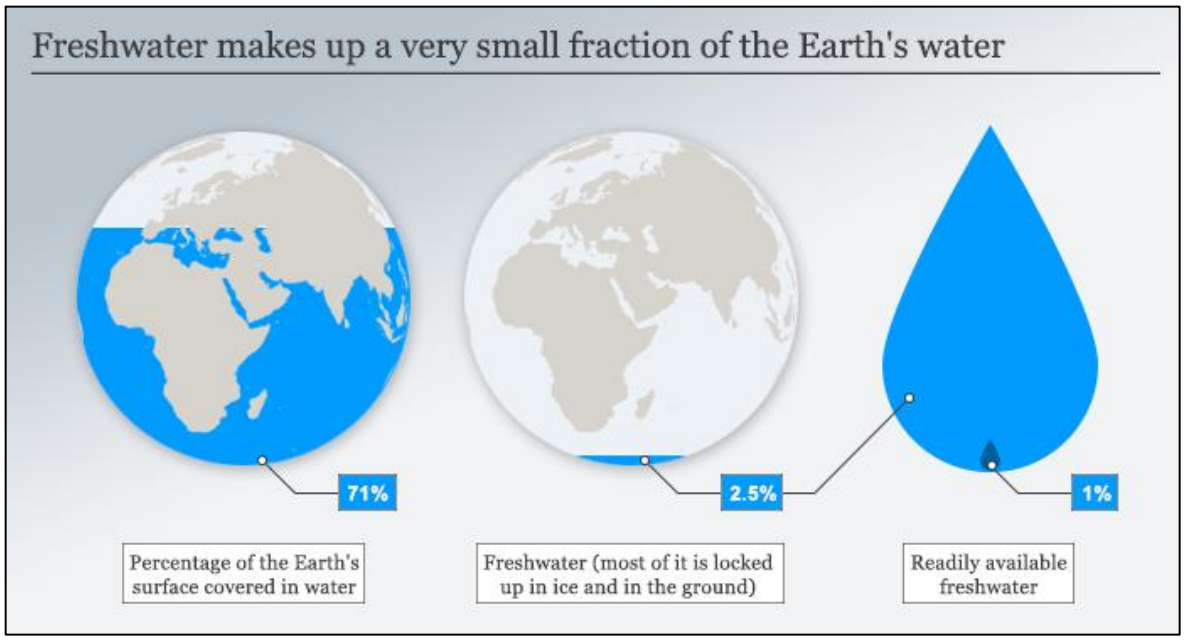

Fig 1: World Water Distribution on the earth [1]

Figure 1 shows the availability of freshwater all over the world. Earth contains 71% water on its surface and only 2.5% water is available as potable water, that too as ice and groundwater, leaving possibly 1.04% readily available potable water for human consumption. And 7.6 billion world population is depending upon this mere percentage of water to drink, cook with, irrigate crops, and feed livestock [1]. Now the issue is, the percentage of freshwater is lessening day by day because of pollution and unwanted uses. Due to inadequate water, the health problem is regularly increasing. Globally, more than three billion people utilize drinkable water origin that is infected from excrement. Infected water can pass on infection such as diarrhoea, cholera, dysentery, typhoid, and polio.

According to the estimation, Contaminated drinking water makes causes 485000 diarrhoeal deaths each year.

Reported Cases And Deaths By Water-Borne Diseases in India										
Disease	2013		2014		2015		2016		2017	
	Cases	Deaths	Cases	Deaths	Cases	Deaths	Cases	Deaths	Cases	Deaths
Cholera	1130	5	844	5	913	4	718	3	385	3
Acute Diarrhoeal Diseases	11413610	1629	11748631	1137	12913606	1353	14166574	1555	9230572	840
Typhoid	1650145	387	1736687	425	1937413	452	2215805	511	1493050	286
Viral Hepatitis	110125	574	138554	400	140861	435	145970	451	98086	283

Fig 2: Different Cases and deaths reported by water-borne diseases In India 2013-2017 [2]

Figure 2 shows the different cases and deaths reported by water-borne diseases in India from 2013 to 2017 while in 2018 more than 1.3 crore people were diagnosed with these water-borne diseases. And 2.2 million cases were reported in 2019. Mostly these cases are reported in remote areas because basic medical facilities are limited in remote areas [2]. Some common water-borne contaminants are carbonates, bicarbonates, and sulfates of calcium and magnesium, fluoride, nitrates, nitrites. In these contaminants, some are very harmful which cause direct death and other cause of diseases.

Figure 3 shows the occurrence of fluoride in the groundwater of Asia. As per the guideline of WHO ingestion of fluoride more than 1.6 mg/l of water brings out dental and bone problems and the ingestion of fluoride in very large quantities for a long time shows highly serious potential skeletal concerns. It is a serious matter, which may have a major problem of incomplete damage to human beings as visualized in Table 1. [5].

Table 1: Influence of fluoride status in freshwater for humans life [5]

Status (mg/l)	**Influences**
1	Raises life of tooth and bones
After 1.6	Refusal body effect
Between 1.6 to 3.8	Shows fluorosis due to yellow and weaken of teeth

Between 4.5 to 8.7	Skeletal fluorosis
9.87	Consumed continuously effects on ruinable fluorosis

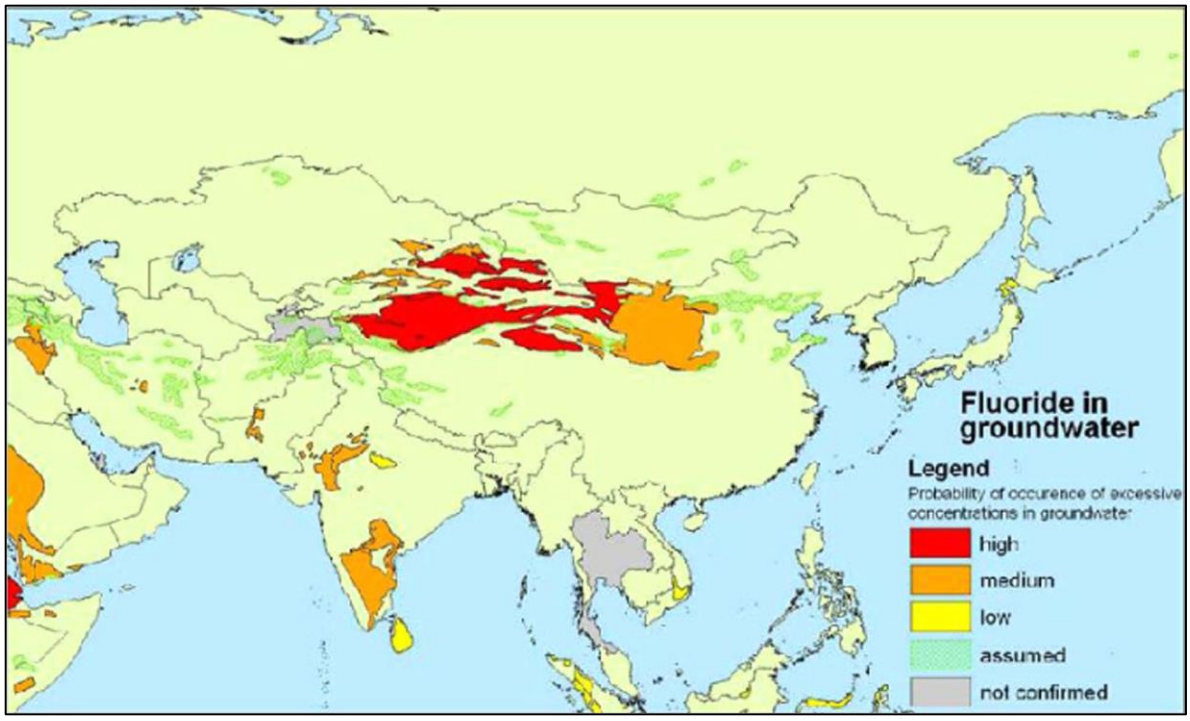

Fig 3: Occurrence of fluoride in groundwater of Asia [5]

Generally, heat is produced from conventional energy producers such as natural gases, oil, and coal. But these producers emit some harmful emissions such as carbon-di-oxide (CO_2), sulfur dioxide (SO_2), and nitrogen dioxide (NO_2). These emissions' effect on global warming may cause cancer and also can produce different harmful diseases The researchers have realized these emissions may also cause of damaging the environment. Therefore, it needs more study on control of using conventional resources There are various ways to turn saline water into freshwater.

Desalination is the best method for removing impurities from water to provide potable water, ultra-pure, or potable water. Some technologies are shown in Figure 3 which are involved in the production of freshwater with the help of different methods by using membrane process (reverse osmosis and non-filtration) and thermal process (multi-stage flash distillation, multi-effect distillation, and electro-dialysis). In these methods, different types of energies could be used in different methods of desalination such as electricity,

solar energy, and fossil fuels. But solar energy is more significant because solar energy has a huge amount of potential and available in abundance [6].

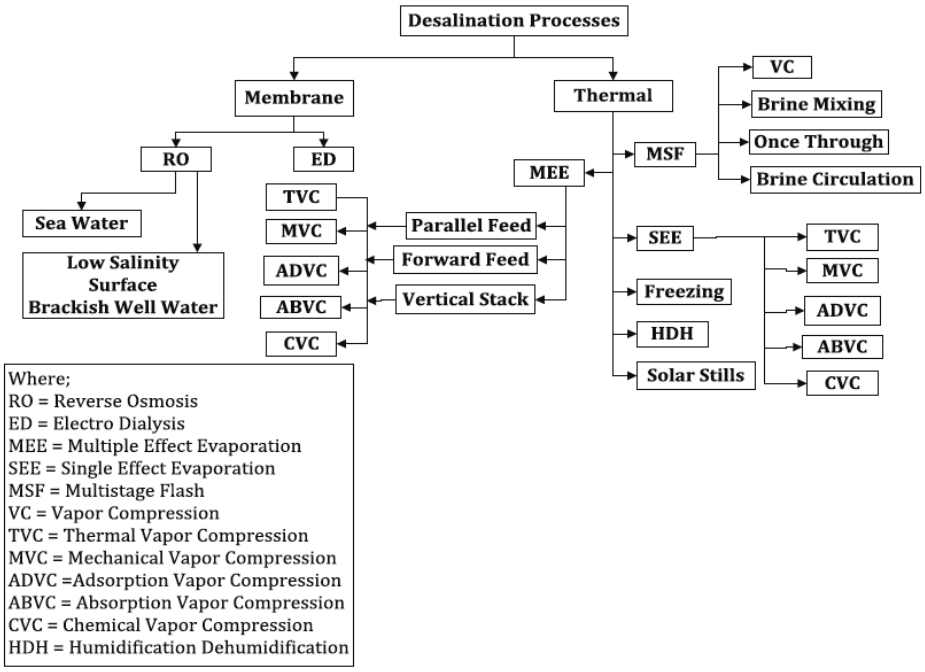

Fig 4: Different desalination processes chart [6]

1.1 Membrane desalination process

Osmosis is a water treatment method in which two liquids are parted by a semi-permeable membrane through which the solvent passes but reduces the motion of dissolved solids. The way of water process depends on meteorological conditions and the number of disintegrated solids. Freshwater has put in on opposite peripheries of the semi-porous diaphragm which shows null in final result inflows of water. If the total number of dissolved solids on both sides has some difference. Then, water will be transferred from the low concentrated mixture to the highly strenuous mixture up to it attains equality. This is a direct osmosis concept [7].

1.1.1 Reverse Osmosis

It is the reverse method of direct osmosis. It is the type of membrane desalination process. In this method, the external pressure is applied greater than osmatic pressure (pressure of more concentred solution). Then the flow of pure water will be towards a less concentrated

solution in the reverse direction. The result shows the globule is held on the higher forced side of the semi-porous diaphragm and freshwater is obtained [7].

1.1.2 Electrodialysis (ED)

This method works on the basis in which the charged particles move in the favorable side of electric flux. Positively charged particles are attracted by negatively charged particles and negative charge moves towards the positive charge outside the electrodialysis cell but in an electrodialysis cell, cations can't cross the semi-permeable membrane. The consequence shows the globule is held with the membrane and pure water is obtained [7].

1.2 Thermal desalination process

Over 55% of freshwater is prepared by the thermal desalination process [5]. In the thermal desalination process, high salted feed water is heated in an evaporator. Boiled ocean water moves through the consecutive divisions with lessening temperature and pressure throughout where ocean water is vaporized and the vapor of water cools for producing freshwater [7].

1.2.1 Multiple-Effect Distillation (MED)

In this method, the system having a sequence of containers (effects) that are kept at lessening states of temperature and pressure with heat transfer ducts. Firstly, ocean water is put into the first chamber where water can be boiled by primary steam. A water fraction vaporizes and both the concentrated ocean water and the flow of the vapor to the succeeding container. In present, the vapor of primary steam cools on the heat transfer ducts, and the remaining heat is forwarded for the next evaporation of the ocean water at less temperature. In the method, the evaporation-condensation process has been used which repeats at each different effect, each state of the system uses the energy released by the foregoing state. At the last effect, concentrated ocean water is released and the left water is permitted to cool in the last condenser [7].

1.2.2 Multiple-Stage Flash (MSF)

Multi-stage flash is found on the concept in which many chambers operate at lessening states of temperature and pressure. In each stage, the heat exchangers pump the water into the next chamber where it is pre-warmed and at last it is forced and heated to the highest temperature with the help of steam from an external device into a brine heater. Then, the first chamber (stage) is kept at a little further down at the saturated vapor pressure of water here. Some parts of ocean water evaporate and strenuous brine moves to the next level where the temperature and pressure are kept a little lessened to prompt high evaporation. This flashing-cooling process is performed again and again from level to level and the cooled water is recuperated at every level by using cooling collectors. The cooling water also flows at each level, drops some of its heat at each stage, and lowers its temperature. Nowadays, it is considered roughly 39 to 46% of the worldwide freshwater is produced by MSF [7].

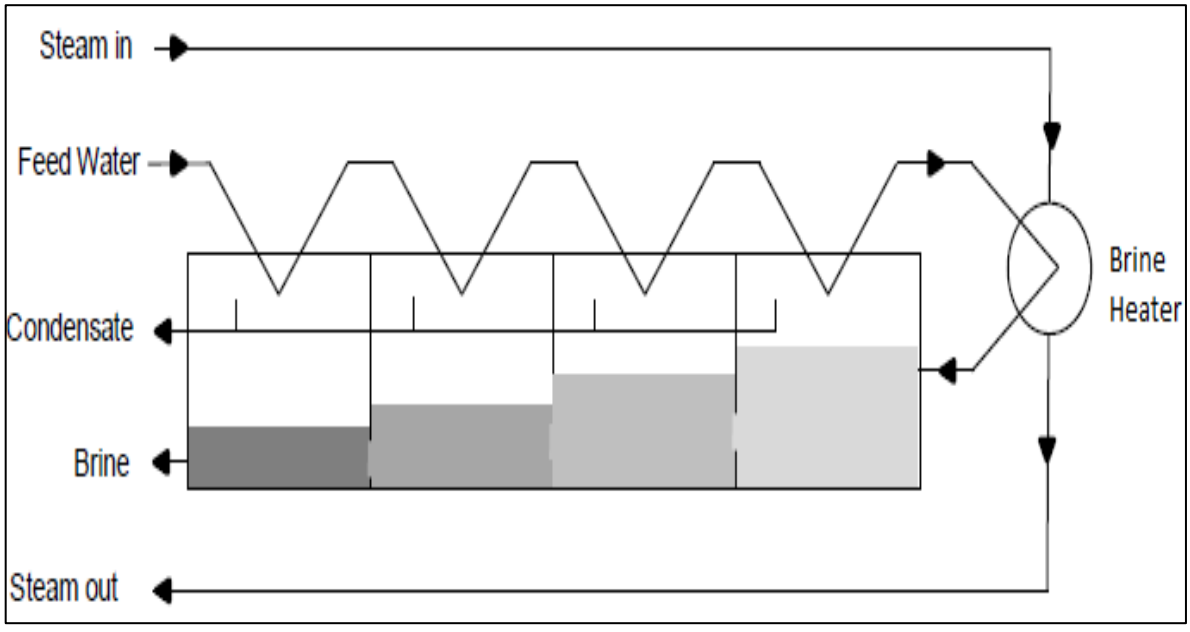

Fig 5: Schematic diagram of multiple-stage Flash (MSF) [7]

1.2.3 Solar Stills

This method uses solar radiation. Solar radiation falls on the earth's surface in large quantities every day, and the distillation of water is done by using these rays. Solar stills are dependent on the concept of the evaporation-condensation method. In this type of method, solar radiations are passed through the glass and then, radiations are taken up by an absorber which raises the temperature of seawater inside the still. Water evaporates and strikes the glass. When solar intensity decreases water tends to condensate on the inner glass surface and to produce distillate water. This method is an eco-friendly and low-cost method and provides drinkable water in remote areas too. Due to providing potable water in remote areas, solar still has become beneficial. Solar still made better using computational fluid dynamics.

The Sun gives us life and energy and is a recent clean non-conventional energy source. India is blessed with a huge quantity of solar energy falls on its surface. In India, it is observed it gains solar radiation for a maximum of 310 days of a year that is about 3000 hr of brightening of the sun in a year. Almost in whole areas of India, each state gains more than sufficient solar radiation. Figure 6 shows the mean solar irradiation in various states of India.

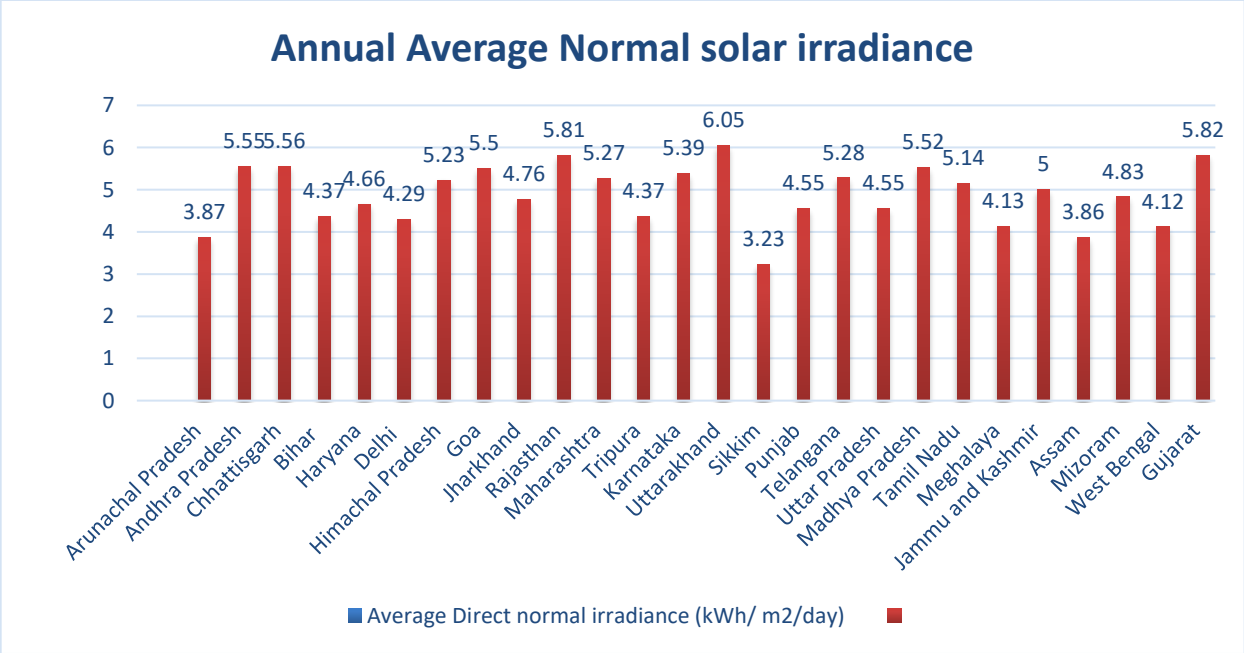

Fig 6: Annual average normal Solar irradiance for various states of India [3]

Figure 7 shows the solar irradiance for each month of the year. The average solar radiation in Delhi is calculated by 4.29 kWh/m^2/day [3].

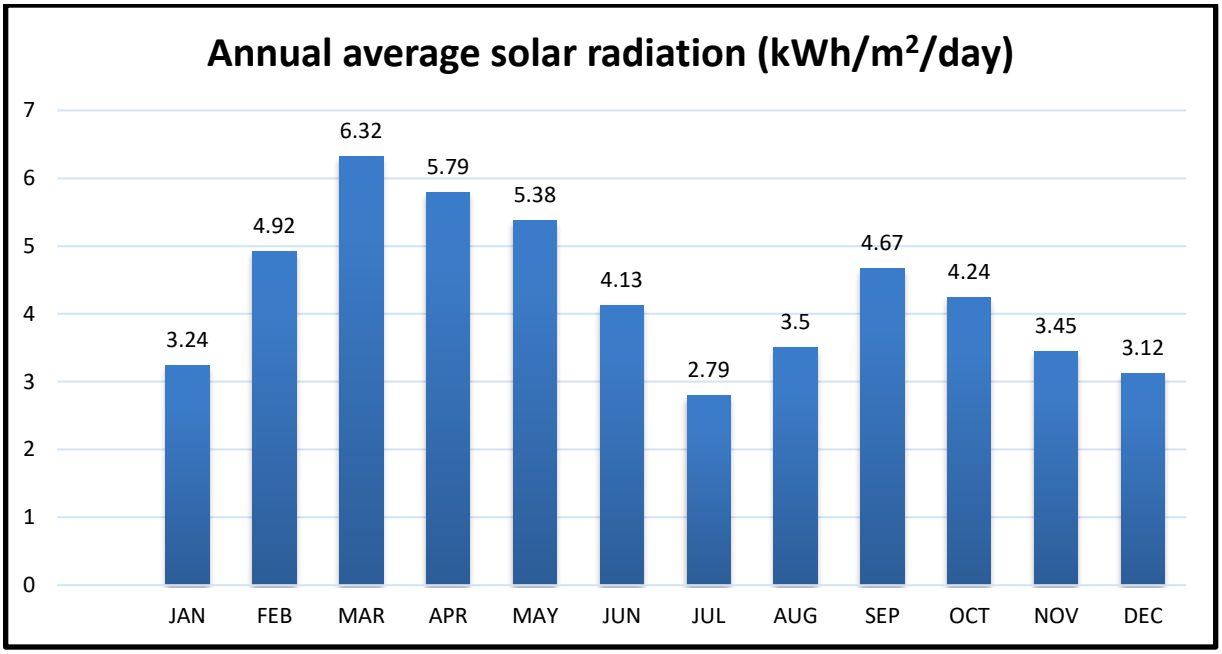

Fig 7: Solar irradiance concerning months [3]

Mostly, the water problem is observed in Delhi very much because of pollution and industrial wastes which make water impure. Even in Delhi, river, and canal all are polluted due to these reasons. Disease in Delhi is regularly increasing due to impure water. Figure 8 shows the different desalination plant installed by the department of atomic energy of Bhabha Atomic energy (BARC). The technologies were given a demonstration and positioned in dissimilar parts of the country and shifted to many parties on a non-restrictive basis. There are some places where the impure water problem is still be held. Today's time, the reverse osmosis system is installed mostly in every house of India but this is a costly method due to which some houses can't buy it and are suffering from diseases [4].

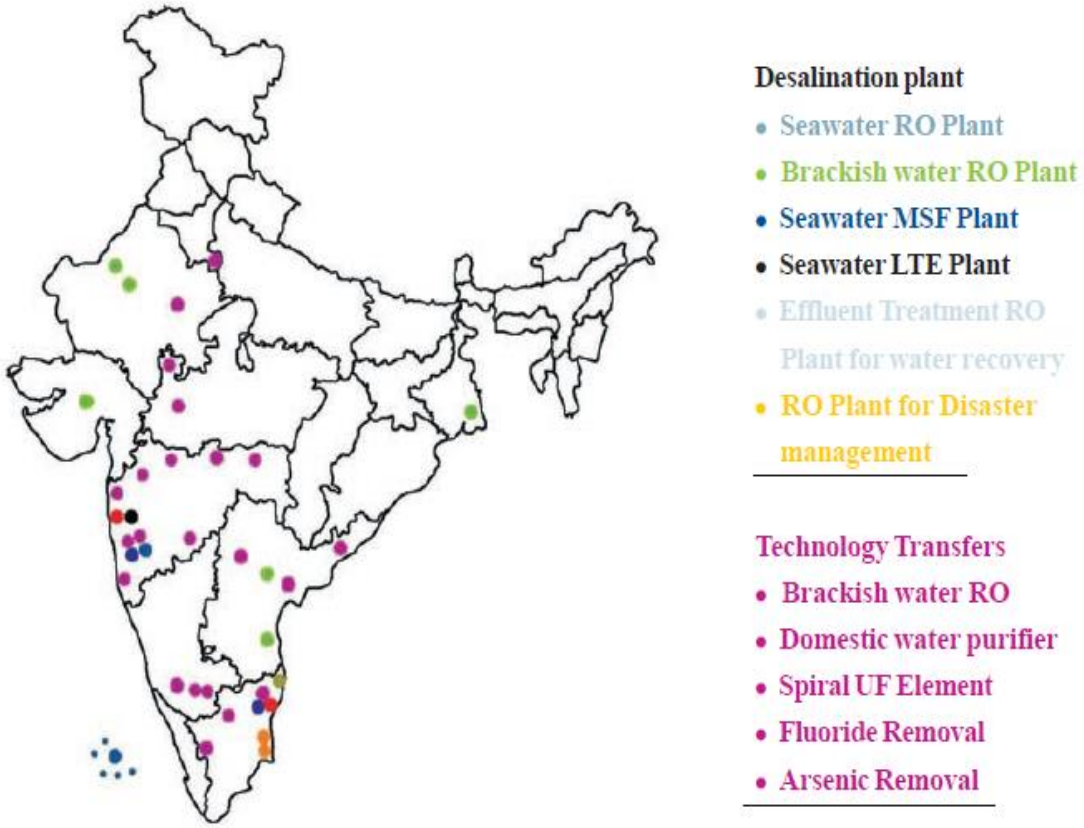

Fig 8: Positioned of desalination and water filtration technologies by the department of atomic energy [4]

CHAPTER 2

LITERATURE REVIEW

Setoodeh et al. [8] developed a three-dimensional model. In this model, a different phase method was used for the combined process of evaporation and condensation by the assist of a computational fluid dynamics simulation tool. By using this tool, a process of the simulation of single slope solar still was accomplished to get results. In the structure of a solar still, the volume of fluid (VOF) was owned to give liquid, and prepared by the combination of the air, water, and vapor system at the quasi-steady-state condition. The building of geometry and meshing was prepared by using ANSYS Workbench 11. A simulation was done by using tetrahedral meshing and different meshing having a different number of elements were developed to calculate better results 32322, 47179, 64694, and 85315 cells. The energy and mass transfer concepts, continuity and momentum at steady-state condition was used for numerical modeling. As a result, it was predicted computational fluid dynamics is a piece of strong equipment for designing process, variables investigation, and can be used for removing difficulties during geometry creating of solar still.

Khare et al. [9] created a multi-phase, 3D computational fluid dynamics model of simple solar still by using ANSYS FLUENT v14.0. and also experimented on it The results of the simulation and exploratory system of single slope solar still were compared with each other for the climate condition of Jaipur. The physical structure surfaces and its meshing was accomplished by the assist of ANSYS Workbench. The meshing of geometry has 3D hexahedral shape elements and 1.5 million elements were created during meshing with a growth rate of 1.2. The energy and mass transfer concepts, continuity, and momentum for the steady-state condition was used for numerical modeling with some assumptions. In a simulation, it was checked the overall efficiency and other parameters.

Panchal et al. [10] performed an experimental and computational fluid dynamics modeling of the single-slope solar still. The Geometry was prepared using ANSYS Workbench 10 and unstructured tetrahedron mesh was used to predict the results. The simulation shows the consequences of water production, water temperature, and heat transfer coefficients using ANSYS CFX 10.

Maheshwari et al. [11] were prepared a geometry of a double slope single-basin solar still, which was modeled by using solid works, and meshing was done using ANSYS ICEM computational fluid dynamics, which consists of 170791 elements. The simulation was done using ANSYS CFX 14.0 to check the production rate and temperature of the water. As a result, it was predicted overall production is maximum in March and November.

Fathy et al. [13] experimented with double-slope single basin solar still which was coupled with parabolic trough collectors (PTC) for increasing heat transfer. The solar radiation incidents upon the parabolic trough collector, which transfers its temperature to the oil finned-serpentine loop heat exchanger. Results of Solar still linked with parabolic trough collectors (PTC) were contrasted from the conventional solar still, which showed the yield of solar still raises by lessening salted water deepness and it also raises by using parabolic trough collectors. The result shows every day pure water outputs at 20 mm salted water deepness is measured 4.51 and 2.31kg/m^2 for conventional solar still and 10.93 and 5.11 kg/m^2 for solar still with parabolic trough collector.

Madhlopa et al. [14] performed research for determining the solar irradiance outflow in single-slope solar still with the help of outside and inside reflectors. In the model, two variables were supposed to estimate, are the reflectance and vision view factor of surfaces. This work was accomplished for single-slope solar still and another for a solar still using a separate condenser. From the results of both still, it was analyzed that conventional solar still produces a maximum value of distillate yield than solar still joined from the condenser.

Panchal et al. [15] experimented for the analysis of different materials of absorber sheets to check the working of double-slope solar still. This experiment was done for increasing the temperature inside the still. It was analyzed that the copper plate has a high value of temperature compared with galvanized iron and a mild steel plate on account of the higher thermal conductivity of copper.

Tripathi et al. [16] performed experimental works to check the influence of different salted water deepness in the container for heat and mass transfer coefficients for single-slope solar still. A variation of heat transfer coefficients with depth was noticed and the internal convective heat coefficient lessens with water deepness because of lessening in temperature of the water. It was observed that the vaporized heat transfer coefficient raised to 0.15 depth.

Badran [17] experimented on single slope solar still. The experiment was acted to evaluate the yield of single slope solar still with the use of asphalt and without the utilize of asphalt. The utilize of asphalt in the basin results in a growth of 29% in output and also remarked that the combination of the sprinkler with the use of asphalt was additional effectual than the use of asphalt.

Singh [18] experimented on single slope solar still and examined it for the finer inclination angle for production. For this analysis, a covered setup was designed at different inclined angles of 15°, 30°, and 45° separately. The consequences of the single-slope still were contrasted with Dunkle's model and data was matched. Consequences give the details that the high evaporation was checked at 45° and the lowest at 15°. The conclusion shows that a rising in inclined angle, vaporization rate, and the temperature difference on either side of the glass inner surface and watering layer increase and have a higher output than Dunkle's model.

Akash et al. [19] experimented with the evaluation of double-slope solar still by using different absorbing materials to raise the production rate of water. To analyze, different absorbing matters such as dyes, ink, and rubber mat were used. The results show that dark dye was the finest absorbing matter and enhancement occurred in output by up to 60%. The conclusion shows that raising the output water of water reduces the effectual isolation region of a solar still, which is a vital drawback in solar purification.

Gokilavani et al. [20] made a model of conventional solar distillation experimentally and also prepared a model by using ANSYS Workbench 14.5 and simulated in ANSYS CFX. The work of the experiment was compared with the simulated study and verified the temperature values over the glass on 27/Nov/2013 and 28/Nov/2013. The result shows the maximum temperature achieved inside the glass and glass temperature on 27/Nov/2013 compared to 28/Nov/2013.

Singh and Mittal. [21] did a simulation of single-slope solar still for obtaining the desired inclined angle to obtain the superior output. The geometry was prepared in ANSYS CAD module and then transferred to ANSYS meshing module for meshing making. Simulation work is completed by ANSYS CFX 13. Boundary condition was used for decoding momentum and energy equation. In the still, two condensing glass covers have 15° and 30° slopes. A simulation was done to get a temperature difference between 40° and 60° at an interval of 2℃ for output. Adhesive forces are used for the evaluation of water spheroid on the glass sheet and 30° inclined to condense cover to get the highest use of heat transfer coefficient of convective and evaporative. The 30° inclined condensing cover provides a maximum production efficiency of 29.4% than 15° slope.

Bhaisare et al. [22] developed a computational fluid dynamics model of double slope single basin solar still for the Gorewada water purification plant, Nagpur. The geometry was prepared in ANSYS workbench and then transferred to ANSYS meshing. The simulation result was obtained by using ANSYS 16.0v. As a result, it was analyzed, the maximum heat flux decreases concerning time, i.e., 9.1054e+005 to 2.0565e+005 in 1 sec and also predicted maximum temperature remains constant and minimum temperature varies with time.

Badusha and Arjunan [23] developed a two-phase 3D structure with the help of ANSYS. Still was prepared for the process of evaporation-condensation in solar still with the help of computational fluid dynamics. It was better by either side of the simulation consequences and the experimental consequences with some misconception. The result estimated using ANSYS CFX shows that it is a potent method for geometry creating, variable estimation, and trouble removal in solar still building.

Thakur et al. [24] accomplished modeling work by computational fluid dynamics tools and experimented with single slope solar still. The geometry was created and then imported for meshing in ANSYS meshing with a minimum grid size of 4 mm and a maximum of 10 mm for achieving better results. The meshing geometry has several nodes 632088 and the total number of elements 553048. The computational work was done for optimizing the different water depths of solar still i.e., 0.01, 0.02, and 0.03 m. and the meshing type was hexahedral. The result is acquired by computational fluid dynamics work and showed better accordance

between exploratory work and simulation work. It was remarked that the optimum depth for the better output was 0.01m.

Sridharan et al. [25] experimented for raising the heat transfer of the double-slope solar still. An experimental layout was prepared for this purpose. This investigated effort was carried out to raise the temperature of the water inlet to the solar still system. To heat the input water a flat-plate collector was utilized in the form of a solar water heater. As a result, in contrast to simple single-basin double slope solar still, there is an addition of a 77% higher yield. To experiment, the water basin depth was kept constant i.e., 2 cm. The theoretical result for simple double slope solar still was 3.55 kg/m^2 whereas the potable water for the active system came out as 4.76kg/m^2.

Panchal et al. [26] experimented and worked on CFD to create a structure of solar still. For raising the absorption of solar radiation, an experiment of single slope solar still was performed that is accompanied by a black layer at the base of the solar still. The simulation of geometry was done in ANSYS CFD 11. The depth of water of the experiment still was 40 cm in clear sky condition. There were four thermocouples used to collect the data. Both simulation and experimental results were compared with each other.

Sampathkumar et al. [27] accomplished a thorough review of single-slope solar still. For enhancing output, a single slope was joined with evacuated tube collector. Accompanied by the collector, solar still works as a merge system. This work was done for different timings of different days. Evacuated tubes coupled solar still provides rising productivity of 77% with temperature increment of about 60℃ than simple still. The conclusion shows There was better accordance between the simulation consequences and the exploratory consequences with some misconception.

Tabrizi et. [28] al did an exploratory analysis on single slope solar still with a built-in sandy tank beneath the basin liner as a storage medium. The integrated heat reservoir produces far up solar still output at the time of the nights and cloudy days. For water injection in solar still, it doesn't need a pumping system. For increasing the accuracy in temperatures, the glass temperature was checked at 12 nodes. The results of solar still visualize that the use of a sandy heat reservoir to a solar basin still increases daily output.

Tripathi and Tiwari [29] worked on a simulation structure for thermal analysis of single-slope solar still by considering the variables of the solar fraction. The geometry of the two-

phase 3D structure was designed in AUTOCAD 2000. The measurements of the system were 1 m × 1 m area with 10.2° slope of the glass cover. The experiment was conducted for New Delhi weather conditions (27.0238° N, 74.2179° E). A MATLAB program was used to calculate convective and evaporative heat transfer coefficients and also estimated sun irradiance. There was better accordance between the simulation consequences and the exploratory consequences with some misconception and theoretical estimation at the time of the day as a contrasting night. In modeling, the following formula for the solar fraction (F_n) for a particular wall of still was used

$$F_n = \frac{solar\ radiation\ on\ the\ wall\ of\ the\ still\ for\ a\ given\ time}{solar\ radiation\ on\ the\ wall\ and\ the\ floor\ of\ the\ still\ for\ the\ same\ time}$$

Tiwari et al. [30] experimented with single slope solar still which was linked with a flat plate collector. A trial was done to assess the temperature of inside and outside glass and influences on yields. A numerical simulation was executed for the weather condition of New Delhi (27.0238° N, 74.2179° E) and also at a height of 216 m greater than the averaged sea status. The variables attached in the investigation were the broadness of cooling casing, collector absorbing surface, wind velocity, and water deepness of the still. Dissimilar condensing cover materials were used whose names are copper, glass, and plastic. The consequence shows that the maximum value of thermal conductivity of copper and minimum deepness are important variables for increasing production. Copper gave higher productivity compared to other materials. The conclusion shows that inside glass temperature shows an important role to estimate production. Per day production is finer for the active system as a contrast to the passive system.

Mishra et al. [31] researched to work for single slope solar still to improve productivity. Different methods and modifications were used for improving productivity. To increase productivity, some additional heat absorbers were added namely gravel, sponge cubes, rubber, glass balls, charcoal, coating absorber aluminum sheet, dyes, and ink in the solar still. The maximum output depends on the surface of the glass sheet, absorber material, and vaporizing layer was 34.7, 40.6, and 7.96 kg $m^{-2}d^{-1}$ individually, and maximum efficiency was recorded 3.5. The conclusion shows that the production of solar still lessens

as it gains in the deepness of water in daylight and also the output of wire-type solar still is roughly 20% more.

Chaibi [32] presented a simulation model of double slope solar still that integrated with a greenhouse roof. The simulation model was prepared for freshwater output and also expressed production variables for water. The numerical simulation was performed for the climate condition of Tunisia and the model was based on heat stability equations which include material layer and brackish water layer. To check the computation of solar radiation, TRNSYS (Transient System Simulation) was taken for simulating the model of solar still. This program shows at each hour calculated solar radiation values for a glass inclination sheet. The influence of solar radiation and optical material belongings are supposed in the system. For solar irradiation calculation, an engineering equation solver (EES) computer was used. The results show that solar irradiation directly influences the regulation of the rooftop- incorporated structure. The vaporizing and optical presentation of the desegregated still greenhouse concept could be modified with the help of the maximization of the solar energy yield.

Ileri et al. [33] performed an experimental work for solar stills to examine the influence of the glass sheet broadness on water production. In these solar stills, three glasses were of 3mm, 5mm, and 6 mm thickness whereas the fourth cover was made up of plastic. Steady flow modeling was prepared for solar still and for getting the result of the equations, a programming software FORTRAN-77 was taken. A numerical simulation was performed for the climate condition of Ankara (40°N,33° E). The results generated by simulation were also contrasted with the results of the experiment and it was remarked that both results have deviated 15%. The simulation was run for 24h and each for 30 experiments. The Newton-Raphson method was utilized to resolve the mathematical model to find the heat transfer coefficients of radiation for glass and water temperature. Efficiency for 3 mm thickness glass was increased up to 26.22 % compared to 5mm and 6 mm. The conclusion shows that addition in glass broadness shows to lessen in output.

Mahendren et al. [34] did a simulation work for double slope solar still to add its production with the help of blending the still water with powdered carbon for getting better productivity. The mathematical model and coding were done by using the MATLAB program for computing the different heat fluxes in the system, to estimate each hour

production of the system and to check the performance of the still. A finalized mathematical investigation was done and different graphs were also plotted in MATLAB. Simulink toolbox was carried out to show simulation. ASCII text files which are M-files were used for coding to enumerate convective, evaporative, and radiative heat transfer rates.

Panchal et al. [35] were done an exploratory on single slope solar still to know the influence of cow dung cakes in the inner side of the basin on heat transfer coefficients and also output. In the single slope solar still, glass cover was inclined at 30° and a water deepness of 0.03m. results visualize about the evaporative heat transfer coefficient is finer than convective and radiative heat transfer coefficients. The conclusion shows that distillate output is better about 25% more in a single slope having cow dung than steel absorber plate single slope without cow dung.

Shukla et al. [36] experimented with an investigation for single slope solar still and galvanized iron used to fabricate the solar still. The vertical and horizontal meshes were also used to raise distillate. The experiment was organized for Maharashtra, India (21.11 ° N, 79.1° E). Results show that both horizontal and vertical meshes raise the freshwater where the horizontal wire-mesh gives average increment distillate output about 400 ml/day and a 6 % increment in the mean filtered efficiency and the vertical wire-mesh provides a notable increment of 13% and 1000 ml per day average distillate output. The conclusion shows that vertical wire-mesh provides better efficiency and produces a high output of pure water.

Nayak et al. [37] did thermal modeling and experiment on double slope solar still. Modified double slope solar still was designed by using transparent acrylic and the north wall of the solar still was fabricated to changed with opaque fiber-reinforced plastic. The experimental geometry was created with the help of CATIA V5R18 software. The simulation result and experimental result was almost closer to each other. The experiment was conducted for Allahabad (25.23°N, 79.09° E) to check the productivity of solar still. Results visualize the modified double slope solar still has 16 kg of freshwater out of 25 kg of brackish water that was formed double than conventional solar still.

Khader et al. [38] experimented with work for upgrading the output of single-slope solar still. Dissimilar modeling methods were taken for intensifying the amount of output.

Different variables were used to increase output. Conventional-type solar still provides a minor output; in consequence, the modification was tried in the current research. The result visualizes that non-transmitting rays lens instead of the consistent basin in solar still, the arrangement guides for the addition of 30%, stepwise basin took to provide a 180% addition in still productivity by the sun-tracking arrangement. The greatest output rate still was achieved at 380%.

The objective of the study is to create a three-dimensional computational fluid dynamics model of single slope and double slope to check the evaporation and condensation processes within solar stills at the climate conditions of Delhi (27.0238° N, 74.2179° E). Both models were developed by using ANSYS Workbench and also simulation works were done with the help of ANSYS FLUENT V19.2. All variables inside both solar still were calculated and examined at each stage. And it is also examined water production of the single and double slope of both systems for the entire day of 21 June 2020.

CHAPTER 3

METHODOLOGY

Two different two-phase 3D models were designed in the volume of fluid of the multiphase phase model. Both stills were also developed using evaporation and condensation processes at transient conditions, which explains the only vaporization of liquid occurred at the surface and their interface was considered for modeling. The act of solar stills depends on different variables such as coefficients of internal heat and mass transfer are checked. The internal heat and mass transfer coefficient in solar still are dependent on convection, radiation, and evaporation. In consequence, the convective heat transfer coefficient, radiative heat transfer coefficient, and evaporative heat transfer coefficient are for the heat transfer coefficient. An RNG k-ε turbulence model was applied with standard wall functions for both phases. The time and volume- average continuity, energy, and mass transfer equations were numerically found in this work for each phase.

3.1 GOVERNING EQUATIONS

Model equations that obey steady-state conditions are dependent on continuity, momentum, energy, and mass transfer conservation concepts.

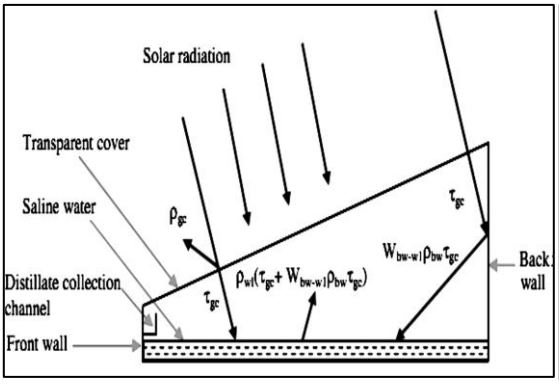

Fig 8. The single slope solar basin [9]

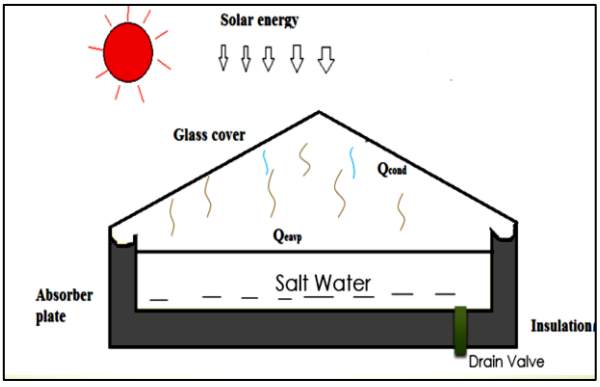

Fig 9. Double slope solar basin [9]

3.1.1 ENERGY EQUATIONS

The assumptions of energy balance equations are:

1. Basin water and glass inside-surface of solar still has no increase in temperature.
2. No escaping of water from any type of hole or crack is present in the solar stills.
3. The water level is kept constant inside the basin.
4. The heat capacity of the glass surface and absorber, insulated material is very low.

The energy equation of the mixture is given below

$$\frac{\partial}{\partial t}\sum_{k=1}^{n}(a_k\rho_k E_k) + \nabla\cdot\sum_{k=1}^{n}\{a_k\bar{v}_k\,(\rho_k E_k + p)\} = \nabla\cdot\left(k_{eff}\nabla T\right) + S_E \quad (1)$$

Where k_{eff} is the effective conductivity $(a_k(k_k + k_t)$,

3.1.2 CONTINUITY EQUATION

$$\frac{\partial}{dt}(\rho_m) + \nabla.(\rho_m\overline{v_m}) = 0 \quad (2)$$

where $\overline{v_m} = \frac{\sum_{k=1}^{n} a_k\rho_k\overline{v_k}}{\rho_m}$

3.1.3 MOMENTUM EQUATION

The momentum equation of all phases is achieved by combining each equation of momentum of all phases.

$$\frac{d}{dt}(\rho_m\bar{v}_m) + \nabla(\rho_m\bar{v}_m\bar{v}_m) = -\nabla p + \nabla[\mu_m(\nabla\bar{v}_m + \nabla v_m^T)] + \rho_m\bar{g} + \bar{F} +$$

$$\nabla.(\sum_{k=1}^{n} a_k\,\rho_k\bar{v}_{dr,k}\cdot\bar{v}_{dr,k}) \quad (3)$$

ρ_m = Density of mixture

$\bar{F}$ = The gravitational body force and external body forces

μ_m= molecular viscosity of the mixture

3.1.4 VOLUME CONSERVATION EQUATION

It is a constraint which shows the unity of volume fractions by adding

$r_G + r_L = 1$ (4)

r_G = volume fraction of gas.

r_L = volume fraction of liquid.

3.1.5 MASS TRANSFER EQUATION

The enthalpy sources in a system for different phases are:

$H_p = -m_p i_q j(h_p^i)$ (5)

$Hq = m_{p^i q} j\left(h_p^i + h_p^{f^i} - h_q^{f^j}\right)$ (6)

3.1.6 PRESSURE CONSTRAINT

The gas phase and liquid phase share the same pressure field

$P_G = P_L = P$ (7)

3.1.7 HEAT TRANSFER EQUATION

The buoyancy force is the main cause of heat transfer. The heat transfer coefficient that has evaporative, radiative, and convective across the contact and the gas phase was prepared with the help of the null equation model and the liquid phase is demonstrated by

$h_{total} = h_{r\omega} + h_{cw} + h_{e\omega}$ (8)

$h_{Cw} = 0.8840(Tw - Tg + \frac{(P_\omega - p_g)(T_w+273)}{268{\cdot}9\times10^3 - P_w})^{1/3}$

where, $P_w = exp\left(25.317 - \frac{5144}{T_w+273}\right)$

where $Pg = \exp\left(25317 - \frac{5144}{Tg+273}\right)$

$$h_{e\omega} = 16.273 \times 10^{-3} h_{Cw} \cdot \frac{P_\omega - P_g}{T_w - T_g} \quad (9)$$

And,

$$h_{rw} = \varepsilon_{eff} \sigma [(TW + 273)^2 + (Tg + 273)^2 (Tw + Tg + 546)]$$

where, $\varepsilon_{e_{ff}} = \frac{1}{\varepsilon_g} + \frac{1}{\varepsilon_\omega} - 1$

3.1.8 WATER PRODUCTION

Defined contact mass flux was used for mass transfer models.

Assumption of water production:-

The rate of freshwater production is equivalent to the rate of vaporization of the water. So, the rate of vaporization of the water shows water production.

Hence, the mass flux equation between the two different phases are:-

$$\dot{m}_{ew} = \frac{\dot{q}_{ew} \cdot A_w \cdot t}{h_{fg}} \quad (11)$$

where,

$$h_{fg} = 2 \cdot 4935 \times 10^6 [1 - 9.4779 \times 10^{-4} T + 1.3132 \times 10^{-7} T^2 - 4.7974 \times 10^{-9} T^3]$$

$$\dot{q}_{ew} = h_{ew} (T_w - T_g)$$

3.1.9 SOLAR IRRADIANCE

$$\delta = 23 \cdot 45 \sin(360 * (n + 284) \,/\, 365)$$

$$\omega = (solar\ time - 12{:}00) \times 15$$

where,

$$Solar\ time = Standard\ time \pm 4(L_{st} - L_{L_0 ca}) + E$$

$$Ig = I_b + I_d \quad (12)$$

where, $I_b = I_{bn} \cos\theta_z$ *and*, $Ig = I_{bn} \cos\theta_z + I_d$

3.2 COMPUTATIONAL FLUID DYNAMICS MODEL OF MODELING

Computational Fluid Dynamics (Computational Fluid Dynamics) is a valuable tool that has been used to examine and inspected the fluid flow repeated method of moisturized air and temperature variation near the walls. For visualizing the flow filed any location computational fluid dynamics can be utilized in preparing the design, getting the controlling step, and can guide. In the study, computational fluid dynamics is utilized to create geometry, and the simulation result is obtained by using ANSYS 19.2v.

3.2.1GEOMETRY CREATION

Ansys is a beneficial engineering simulation software that is mostly used for solving engineering problems and also to make them more optimized. Figure 10(a) and figure 10(b) show the 3D geometry of single slope and double slope solar still, which were modeled using Ansys Design modeler in Ansys 19.2.

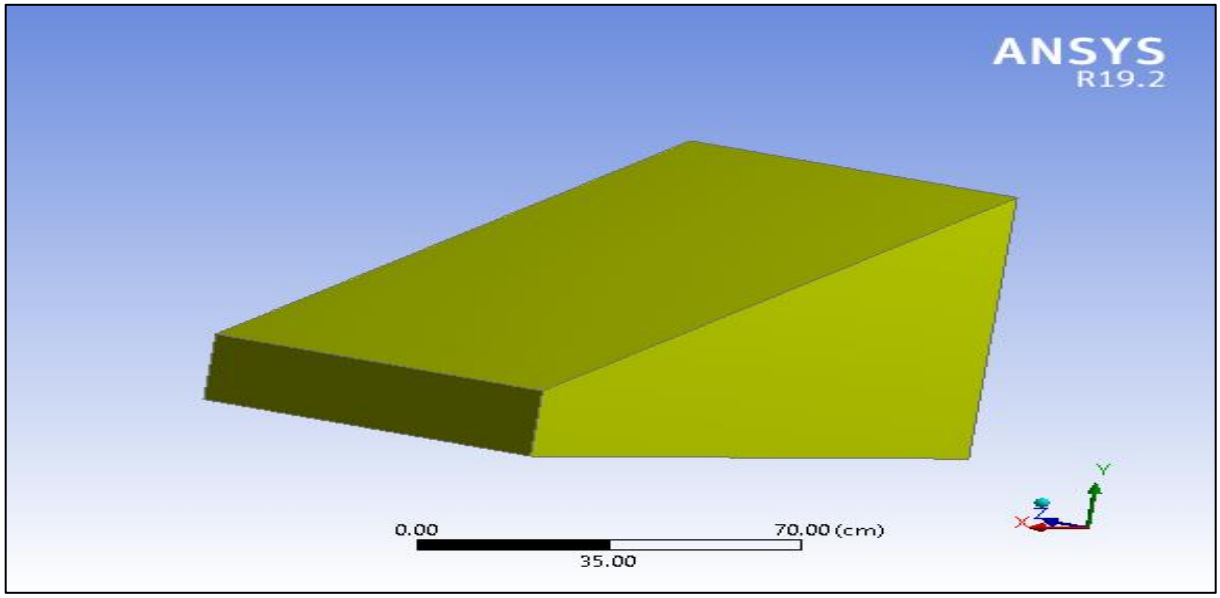

Fig 10(a). Single Slope Single Solar Still.

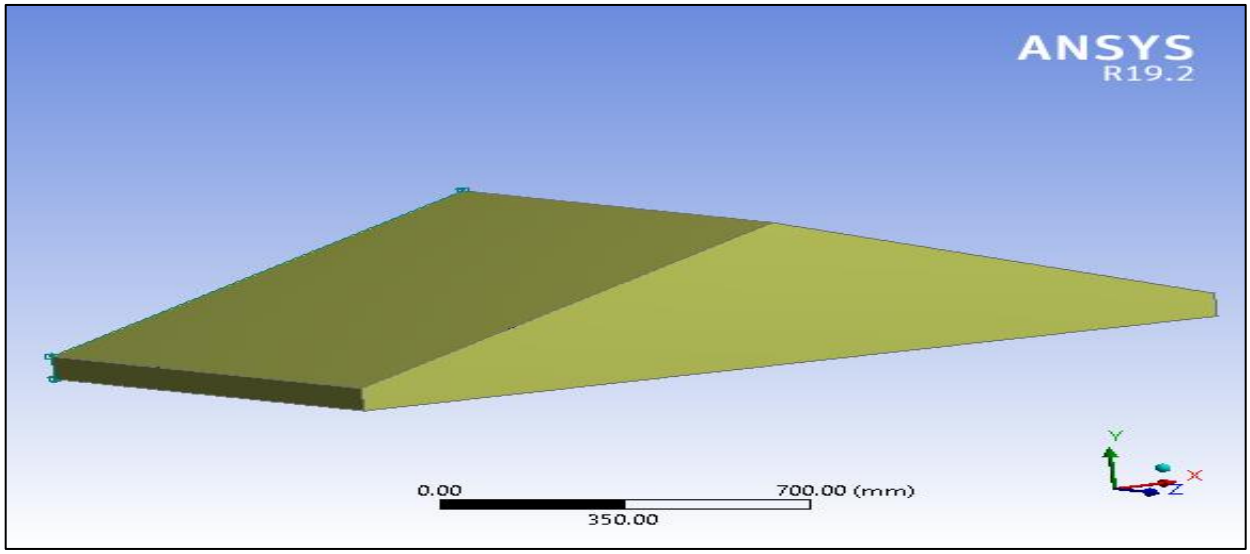

Fig10 (b). Double Slope Single Solar Still.

Both stills contain different parts like absorber, sidewalls on both sides, front wall, back wall, and collector (single collector in single slope and double collector in double slope) are modeled as per the dimensions.

3.2.2. MESHING

The physical model of both systems then, meshed by using ANSYS 19.2 workbench Meshing. Fig 11(a) shows an unstructured mesh of single slope solar still, which consists of a total of 545000 elements and 566610 nodes at a growth rate of 1.2 and element size 10mm using 3D hexahedral meshing.

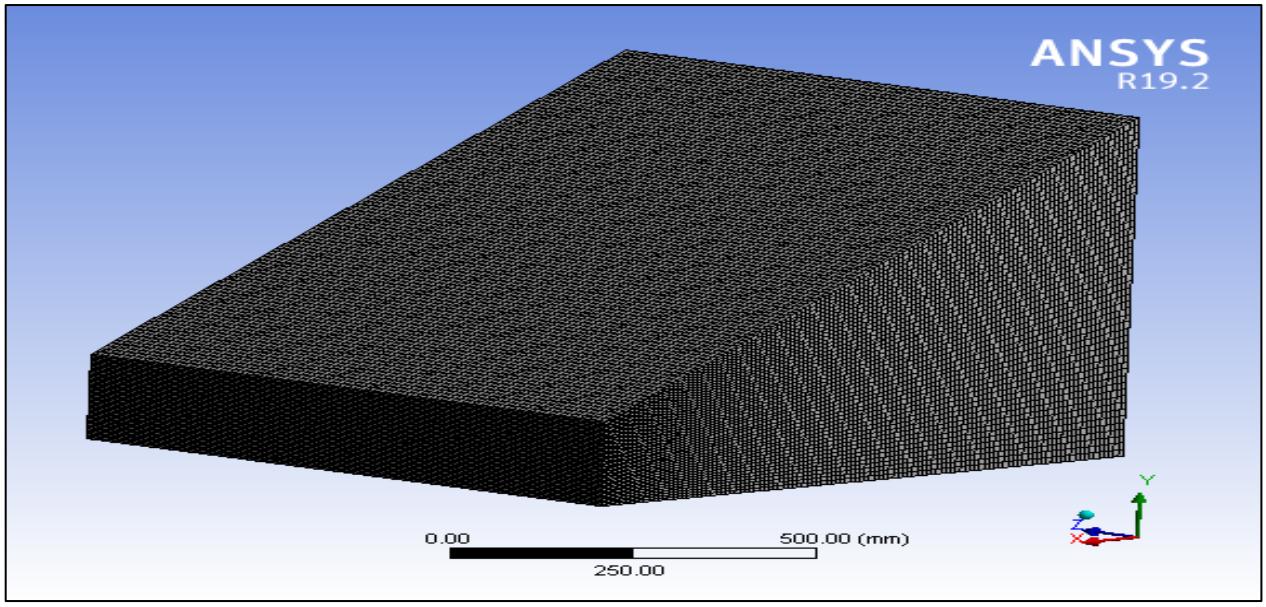

Fig 11(a). The unstructured mesh of single slope.

Fig 11(b) shows an unstructured mesh of slope solar still, which consists of a total of 586200 elements and 612464 nodes at a growth rate of 1.2 and element size 10 mm using 3D hexahedral meshing.

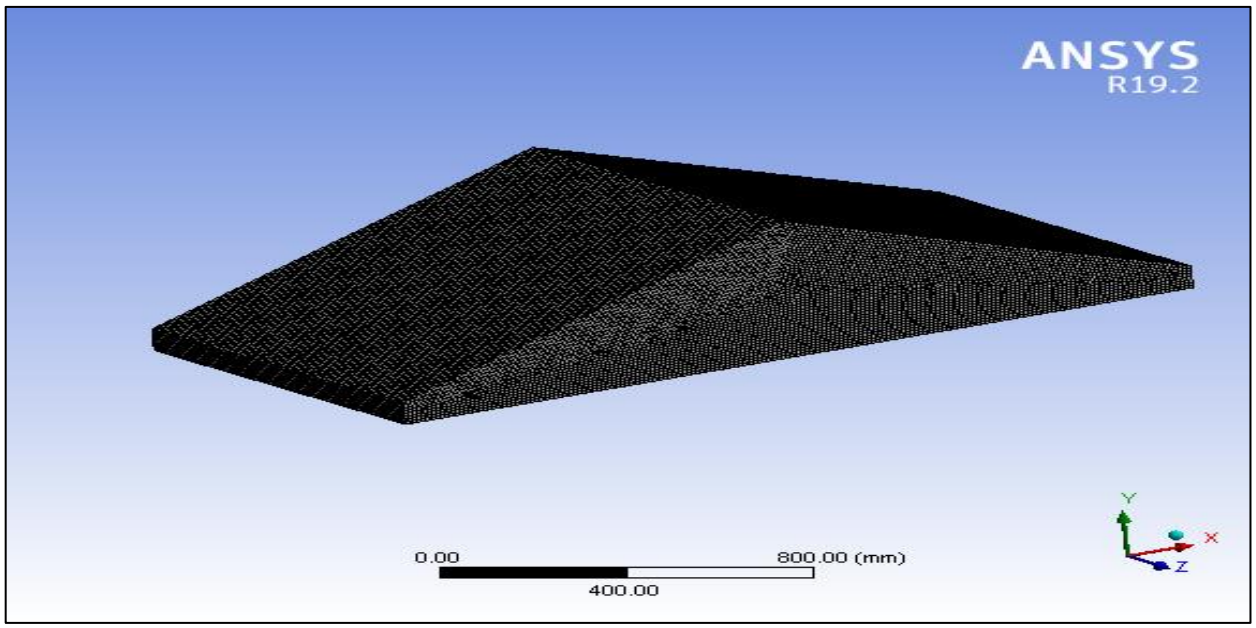

Fig 11(b):- Unstructured mesh of double slope still.

3.2.3 BOUNDARY CONDITIONS AND INITIAL CONDITIONS

Meshing files of both solar stills are transferred to ANSYS FLUENT. A multiple phase structure of both solar still was prepared in the volume of fluid (VOF) framework for liquid water and a mixture of air and water vapor system at the transient condition with gravitational acceleration. Solar irradiance falls on solar stills is an important element for the inner side of solar stills, which are dependent on the absorptivity and transmissivity of the glass cover. First of all, solar rays are falls upon the surface of the glass and then absorbed by an absorber sheet, and raises the value of the temperature of the water. In the fluent, physics and boundary conditions are specified to solve the continuity equation, momentum equation, and energy equation at all the boundaries. The RNG k-ε viscous model was used, which predicts the spreading rate of flow and better performance of water production. In the model, the near-wall conditions were dealt with using 'standard wall function". Adhesion forces are taken for producing droplets inside the solar stills. No-slip wall boundary conditions were defined for both gas phase and liquid phase. the volume fraction of the water and air were taken as 0.13 and 0.87. Computational fluid dynamics simulation had run time of 5 hours for single slope solar still and 6.30 hours for double slope solar still.

Table 1: Boundary conditions for the simulation process of single slope and double slope

Domain	**Domain type**	**Location**	**Boundary type**	**Boundary details**
Solid	Cell	Absorber plate	Wall	Stationary wall with heat flux
		Glass cover	Wall	Fixed wall Temperature
		Sidewalls	Wall	Adiabatic
		Front and back wall	Wall	Adiabatic

CHAPTER 4

RESULT AND DISCUSSION

In this study, simulation results were calculated at fair weather conditions, and each stage of both stills using ANSYS FLUENT v19.2. In Simulation results, the temperature distribution inside both stills is examined and predicted the temperature of both stills for the entire day.

4.1 SIMULATION RESULTS

ANSYS FLUENT v19.2 was taken to check the results by using 3 GHz CPU processors as parallel run with double precision. Fluent uses a second-order upwind solution method to transform the governing equations into a numerically solvable algebraic equation.

4.2 TEMPERATURE DISTRIBUTION

Fig. 12(a) and 12(b) respectively visualize the gas-phase temperature volume rendering inside the single-slope solar still and double slope solar still. Temperature variation at each stage was calculated inside the stills. In the temperature volume rendering, the red color visualizes the maximum value of the temperature, while the blue color visualizes the minimum value of the temperature for both stills. In a single slope, the temperature is increasing from bottom to top slowly while in double slope solar still, the temperature is increasing rapidly from bottom to top. Both stills are attaining maximum temperature at the top because of the orientation of the mesh towards solar incident rays.

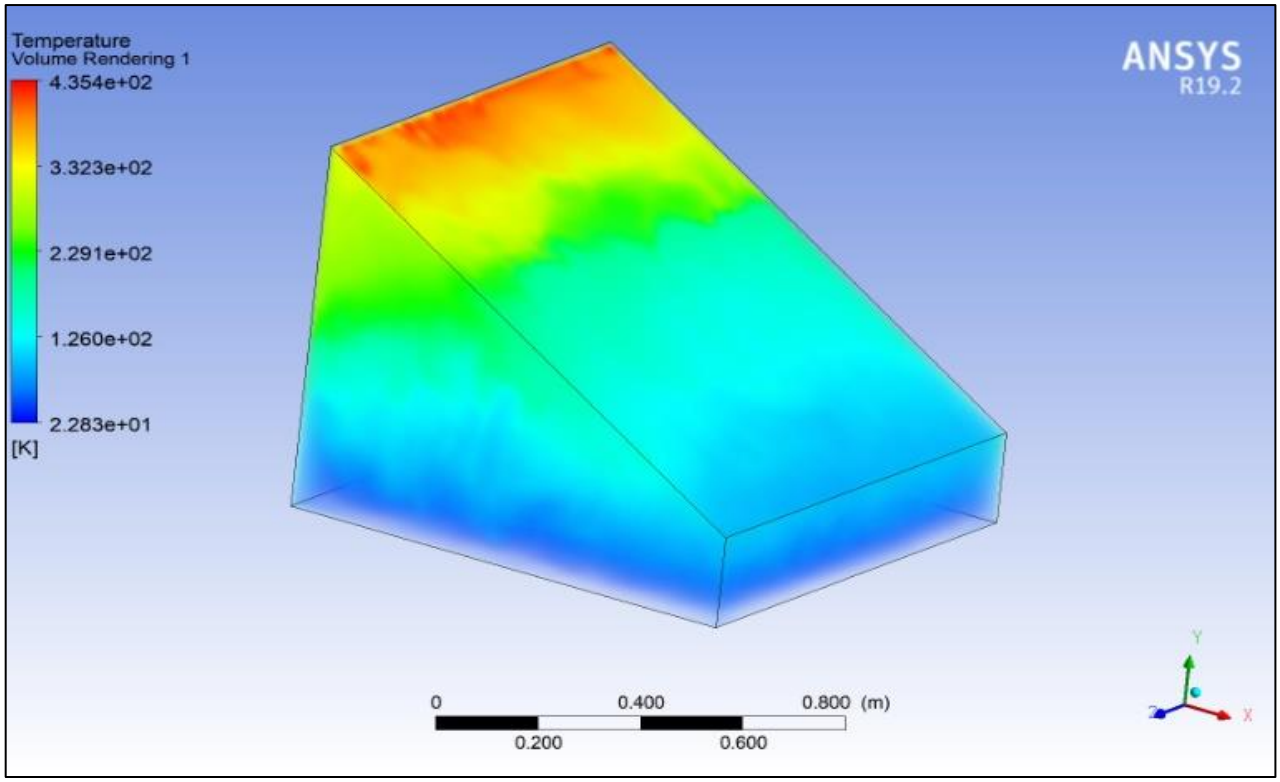

Fig 12(a). Temperature distribution inside the single slope solar basin.

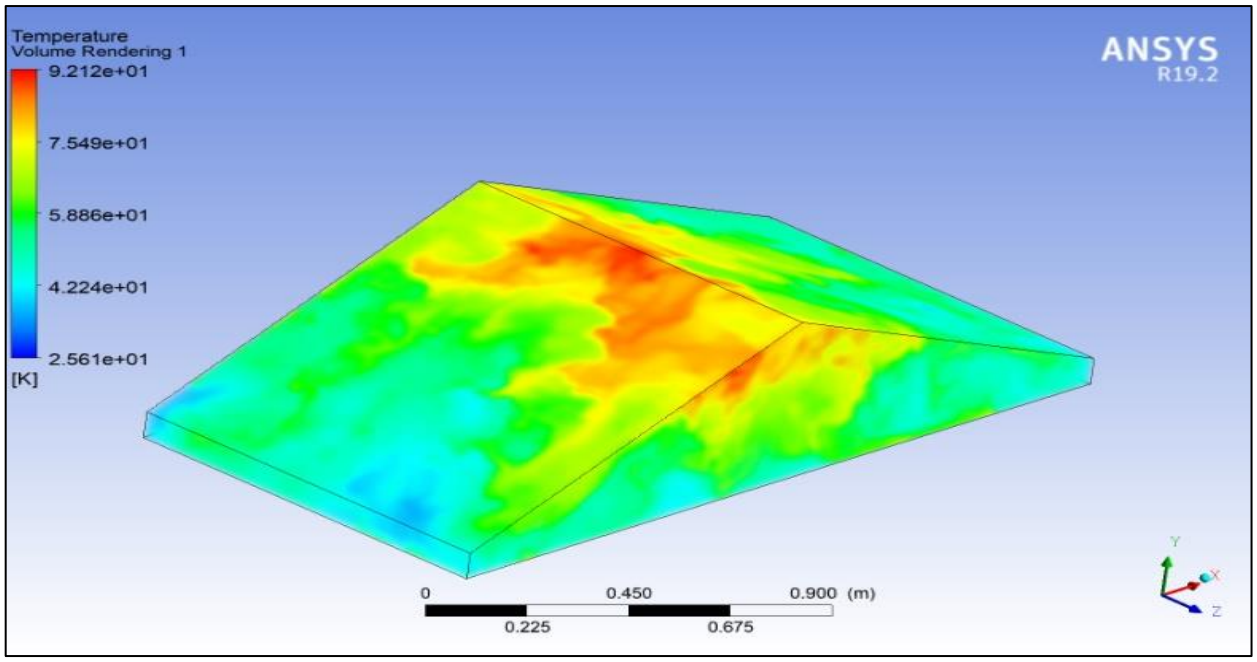

Fig 12(b). Temperature distribution inside the double slope solar still.

4.3 TEMPERATURE VARIATION WITH TIME

Figure 13 shows the temperature variation of single slope solar still concerning the time. The temperature of the single-slope solar still is calculated for the entire day. From the simulation result, it was predicted the maximum temperature was obtained at 13:00 hr. i.e., 435.99 K and while the minimum temperature is obtained in the morning during sunrise and sunset i.e., 22.283 K, which is the very low temperature to convert the water into vapor. The red line in the graph shows the temperature while the blue line shows time on the streamline. From the graph of a single solar still, it is predicted that there is no time when the temperature inside the single solar still is constant (Fig.13).

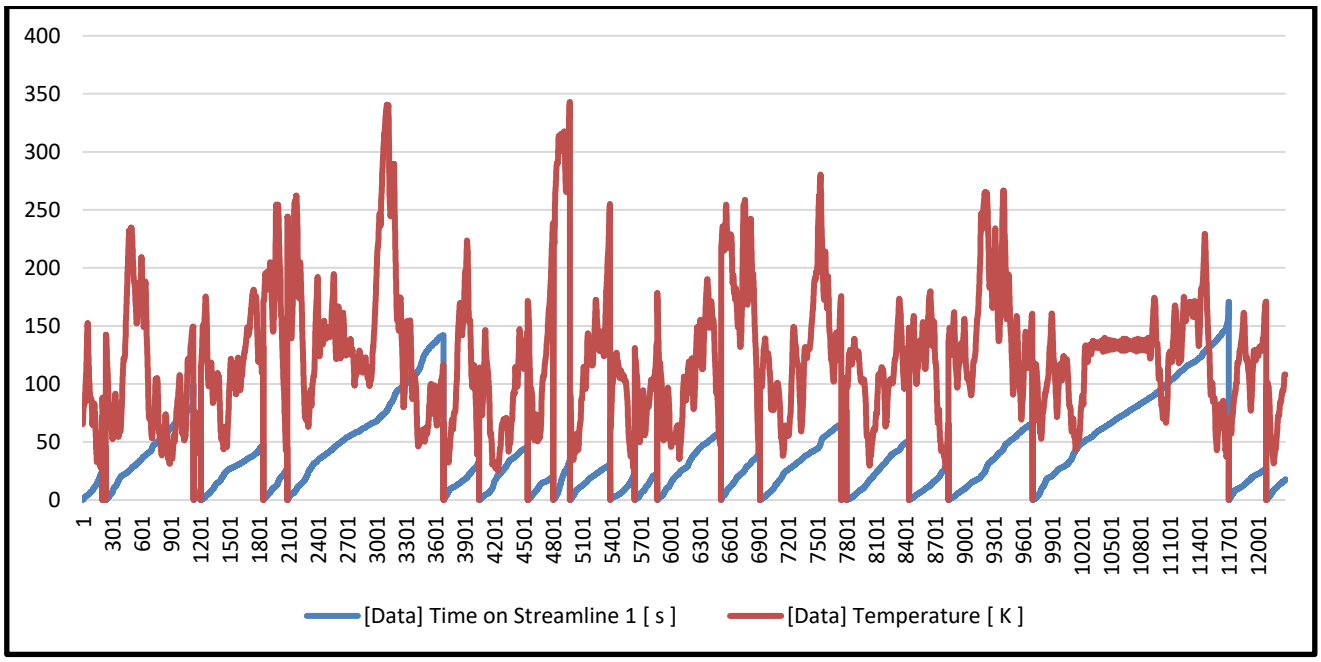

Fig 13. Temperature variation concerning the time of single slope solar still.

Figure 14 shows the temperature variation of the double slope solar still concerning the time. The temperature of the double slope solar still is also calculated for the entire day. From the simulation result, it was predicted the maximum temperature was obtained at 13:00hr, i.e., 92.1204 K and while the minimum temperature is obtained in the morning during sunrise and sunset, i.e. 25.6081 K. The red line in Figure 14 shows the temperature while the blue line shows time on the streamline. From the graph of a single solar still, it is predicted that temperature is almost constant from 12:00 to 12:30 hr. Then, it increases,

and at 13:00 hr. it attains maximum temperature. Again, from 14:00 to 14:15 hr., the temperature is almost constant, and it decreases.

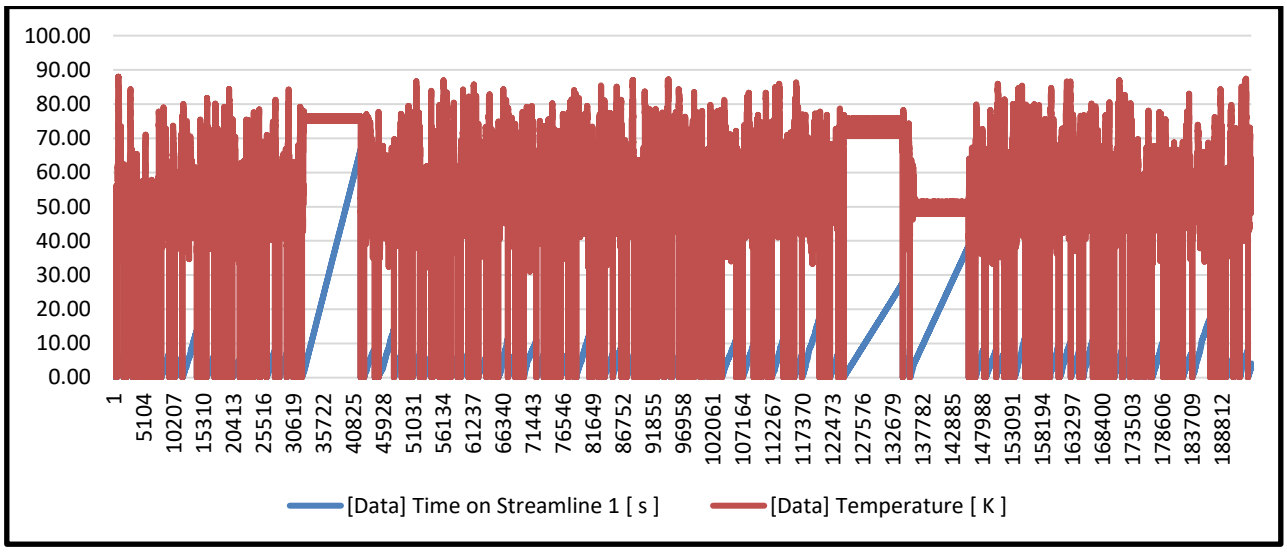

Fig 14. Temperature variation concerning the time of double slope solar still.

4.4 WATER VOLUME FRACTION

The volume fraction of the water contour having the side view of the system is visualized in Figure 15 in which blue color is allow to visible less volume fraction of water, while red color shows more volume fraction of water. The volume fraction of water is increasing from top to bottom inside the still and it is observed maximum volume fraction is near absorber, i.e 0.0183968 and minimum 1.8773×10^{-6}.

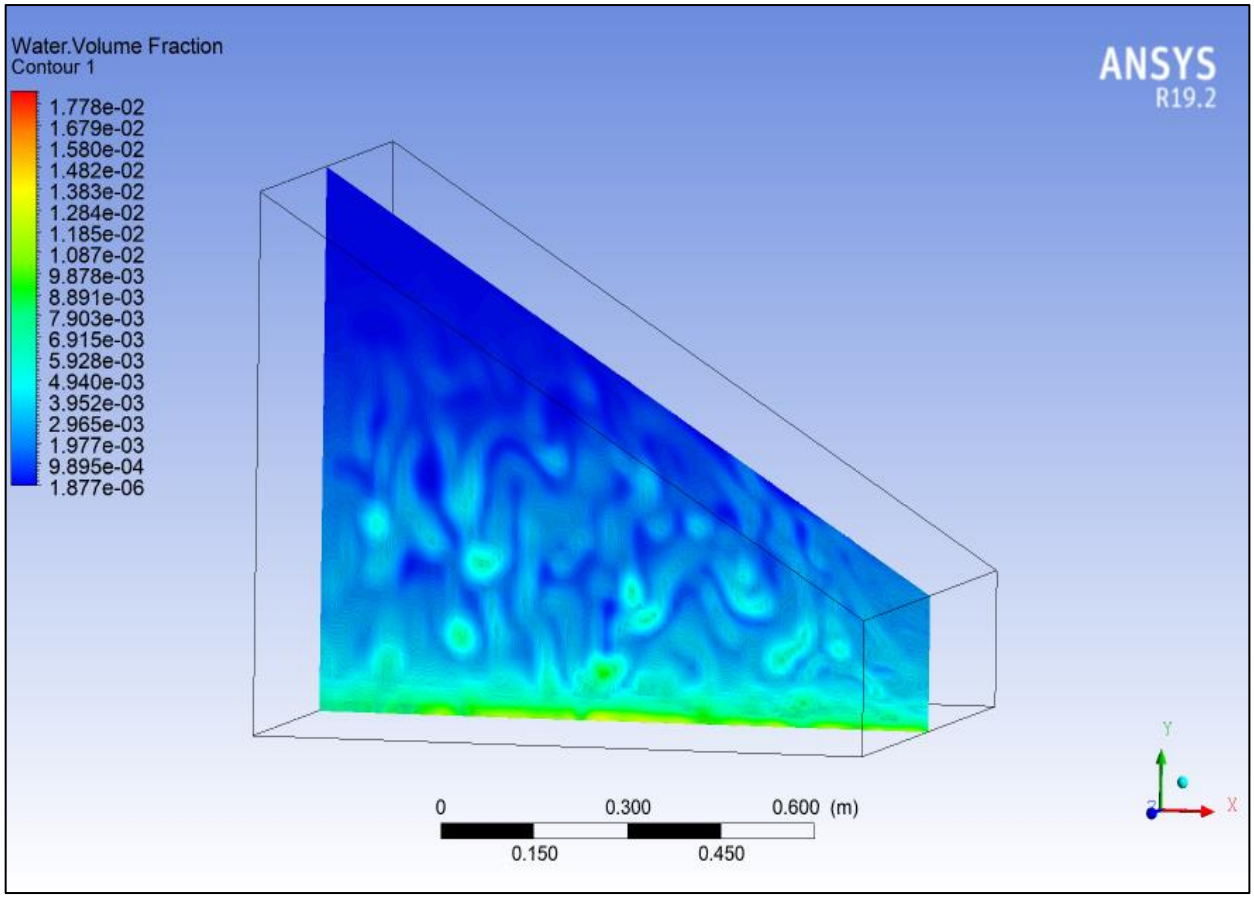

Fig 15: - Water volume fraction contour inside the glass of single slope still.

Cooled water on the glass is visualized in Figure 16. It is observed volume fraction of droplets on the inside of the glass surface in contrast to its surface is less. Water volume fraction contours having the glass surface view of the system are shown in Figure 16 in which the blue color is visualizing a reduced value of the volume fraction of water whereas the red color is visualizing more volume fraction of water. The volume fraction of droplets is increasing downward on the glass. The maximum value of the volume fraction of water on the glass is 4.94×10^{-3}.

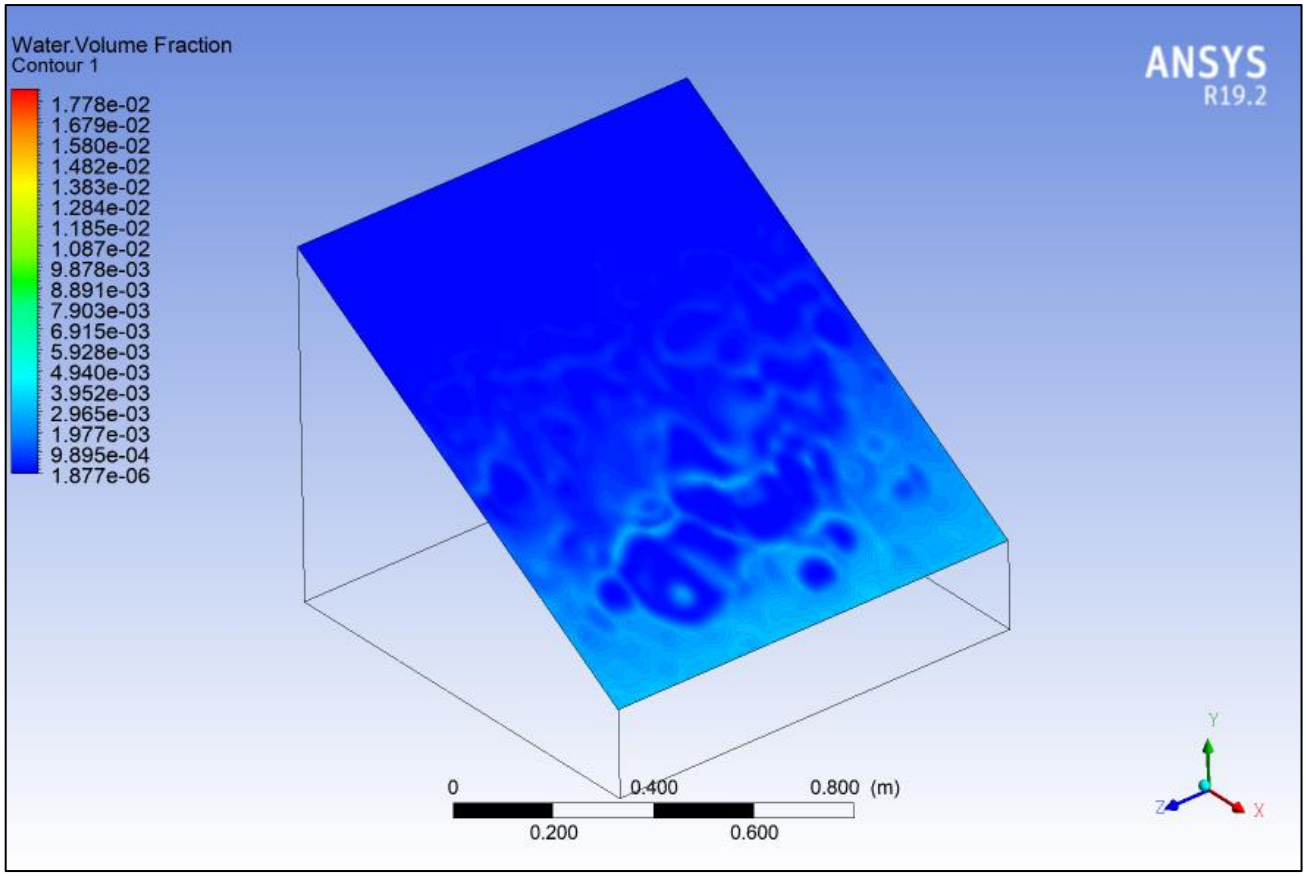

Fig 16: - Water volume fraction contour on the glass of single slope still.

It is also detected in double slope still, the volume fraction of drops of water on the glass in contrast to the surface is low. The volume fraction contours of the water having the glass surface visibility of the system are shown in Figure 17 in which the blue color is visualizing less amount of the volume fraction of water, while the red color visualizes more volume fraction of water. The volume fraction of droplets is increasing downward on the glass. The maximum water volume fraction on the glass is observed 0.01692 and a minimum 0.00130. It is predicted that the water volume fraction of glass of double slope is higher compared to glass of single slope.

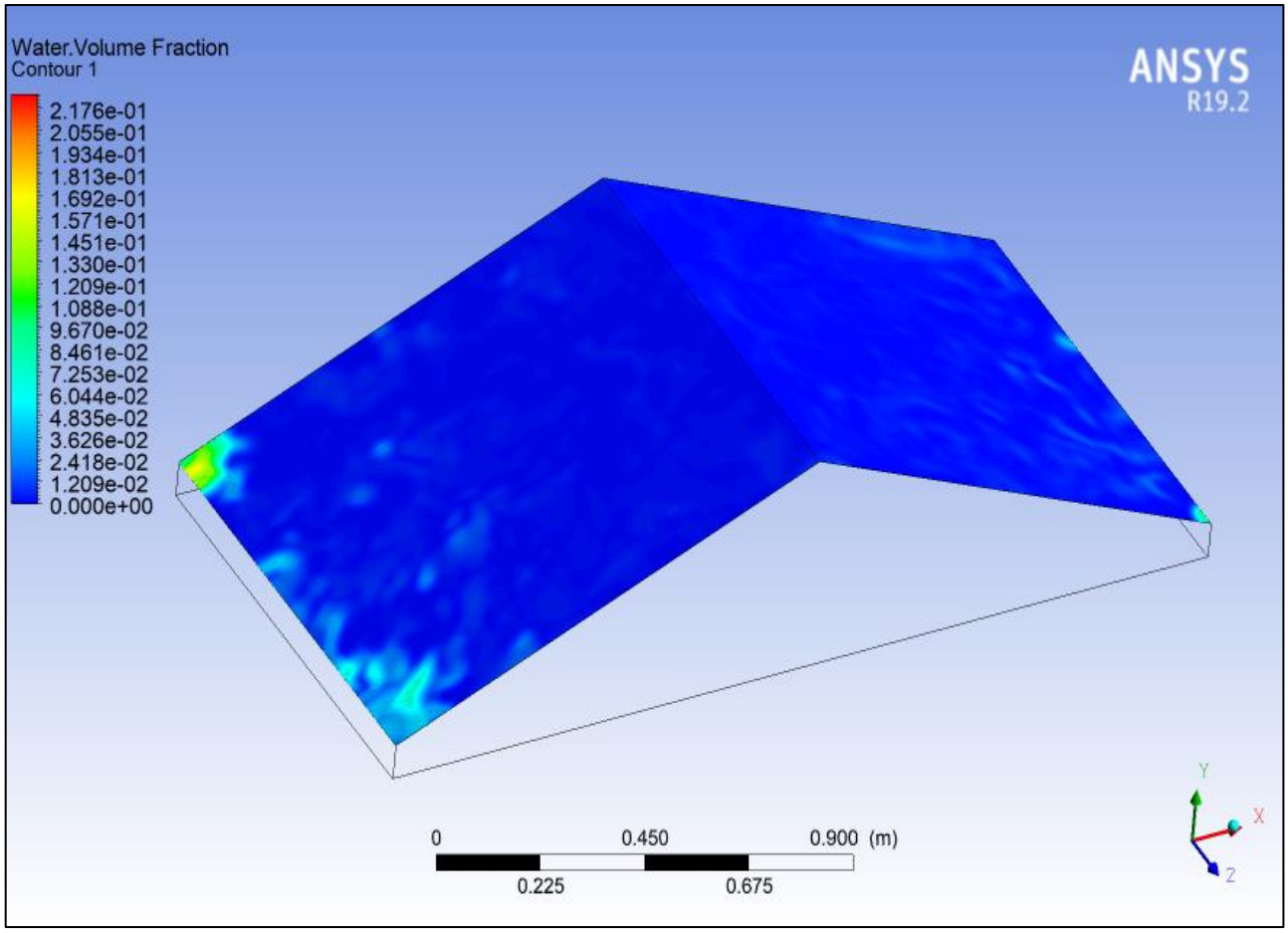

Fig 17. Water volume fraction contour on the glass of double slope still.

The volume fraction contour of the water having the side view of the system is shown in Figure 18 in which the blue color is visualizing less the value of volume fraction of water, while the red color visualizes more volume fraction of water. The value of the volume fraction of water is increasing from top to bottom inside the still and it is observed maximum volume fraction inside the double slope is 0.225132 and the minimum 1.8773×10^{-6}.

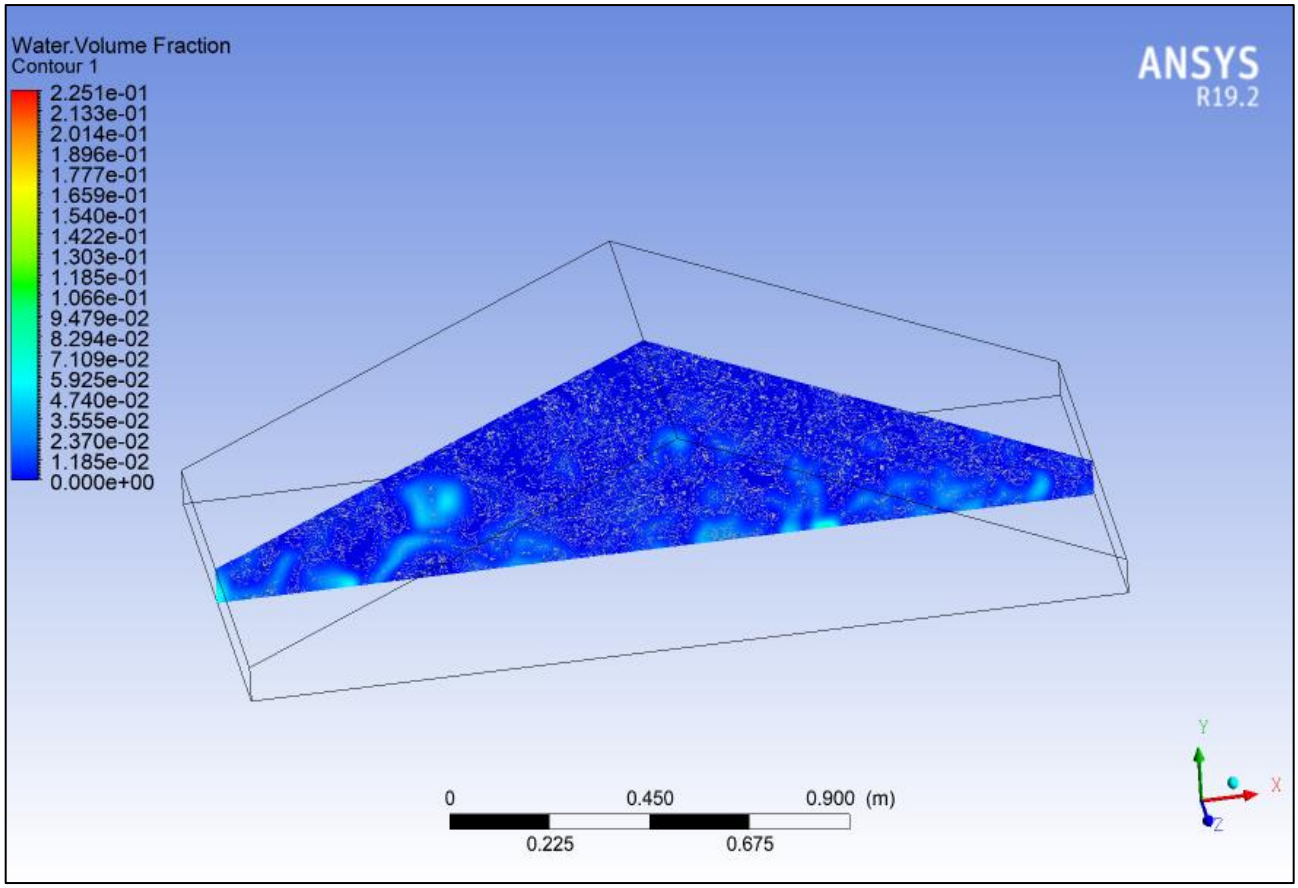

Fig 18. Water volume fraction contours inside the glass of double slope still.

Volume fraction contours of the vapor having the side view of the system and glass view are visualized in Figures 19a and 19b in which blue color shows less volume fraction of vapor, while red color visualizes more volume fraction of vapor. The volume fraction of vapor is decreasing from top to bottom inside the still whereas, on glass, the vapor volume fraction is increasing downward of glass. It is observed maximum volume fraction of vapor is 0.999998 and a minimum 0.871514.

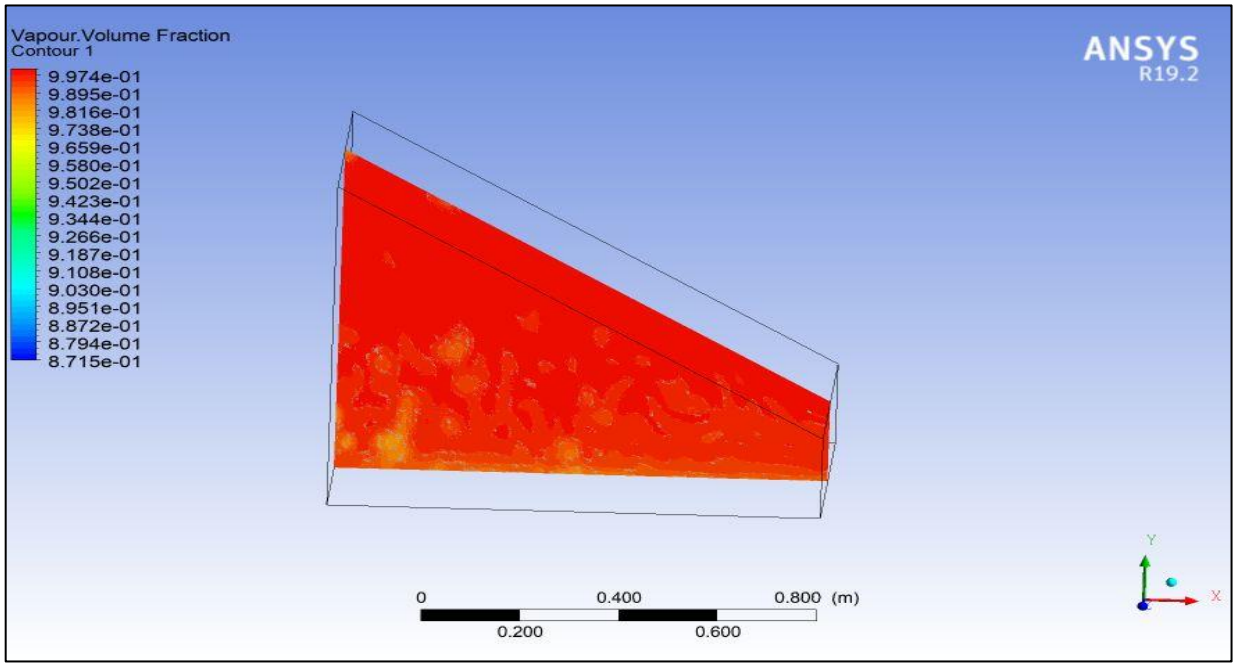

Fig 19a. Vapor volume fraction contour inside the single slope solar still.

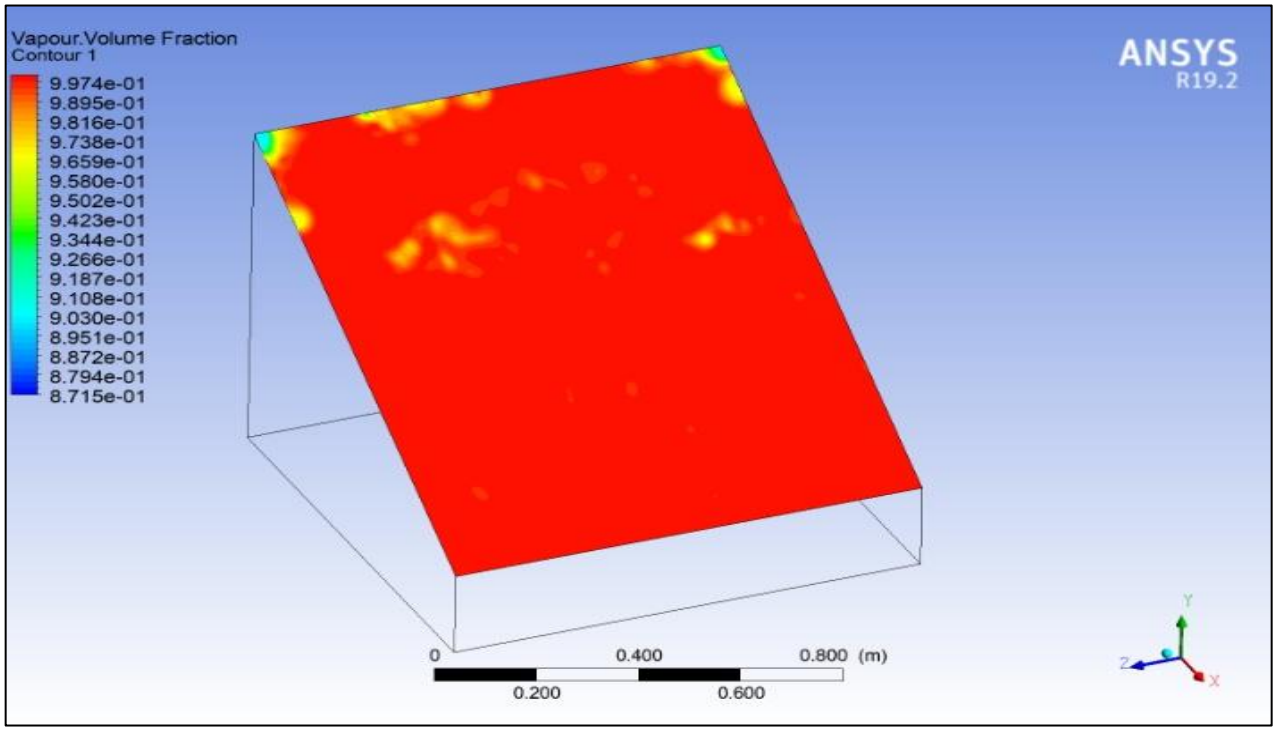

Fig 19b: - Vapor volume fraction contour on the glass of single slope solar still.

Vapor volume fraction contours having side view and glass vision of double slope still are shown in Figures 20a and 20b. The maximum vapor volume fraction in the double slope is 0.999999 and the minimum is 0.000917328. From both stills, it results that the maximum water volume fraction can be achieved in double slope still, whereas the maximum value of the volume fraction of vapor can be achieved in a single slope still.

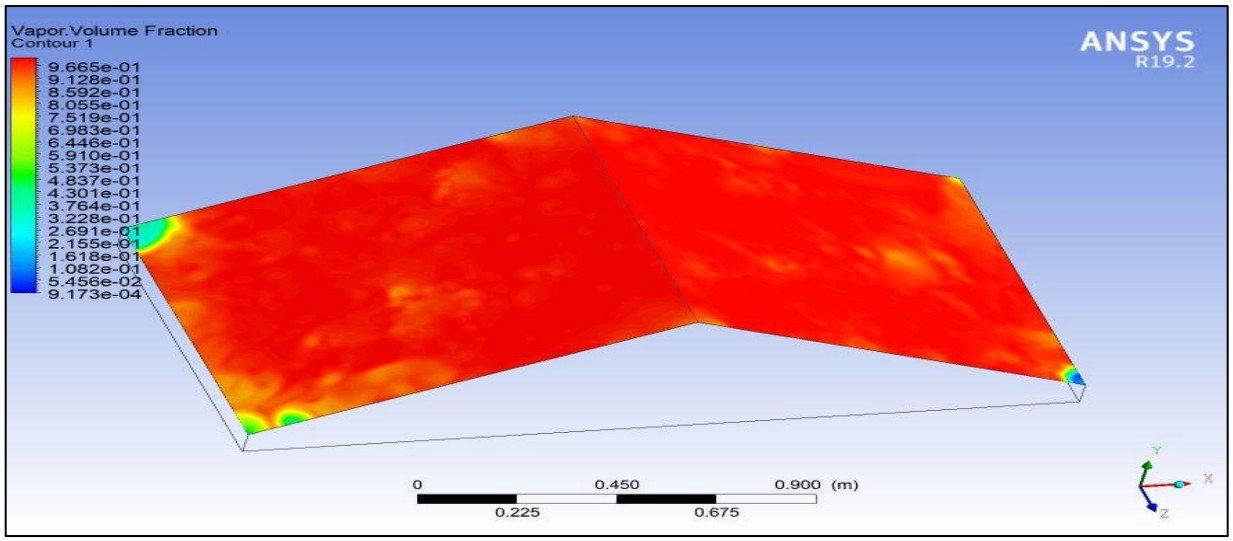

Fig 20a. Vapor volume fraction contour on the glass of double slope solar still.

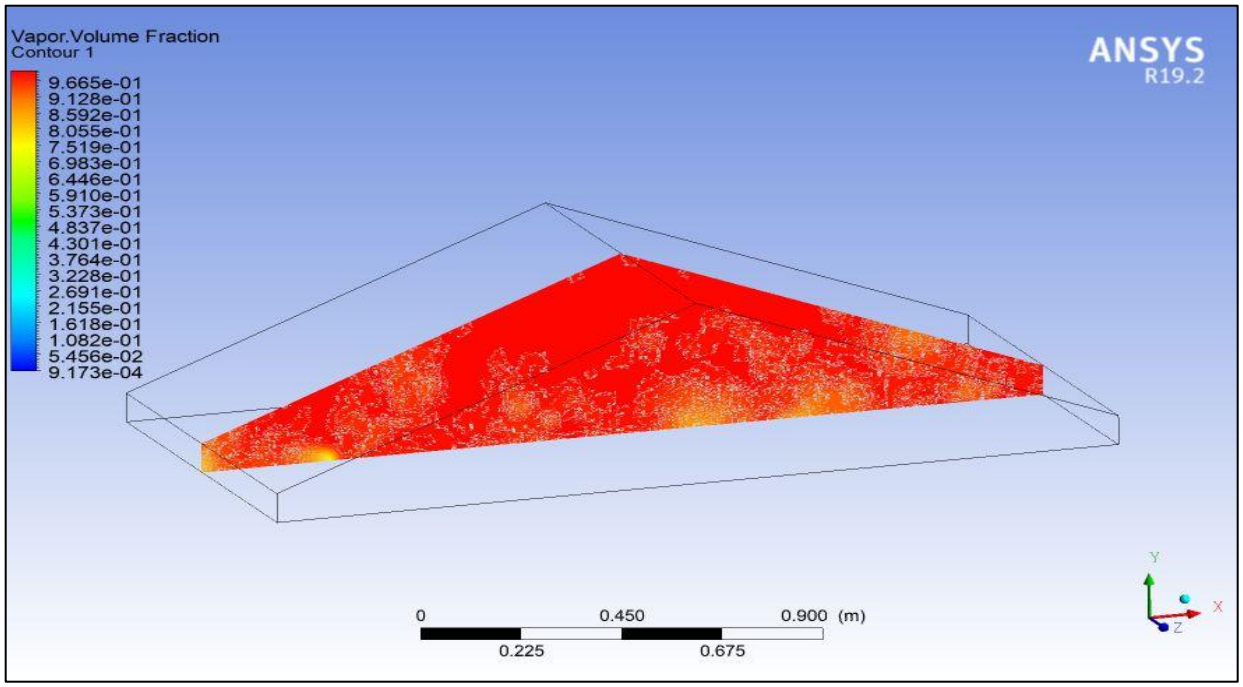

Fig 20b. Vapor volume fraction contour inside the glass of double slope solar still.

Figure 21 visualizes the volume fraction of water of single slope solar still concerning the time. The water volume fraction of the single-slope solar still is calculated for the entire day. From the simulation result, it was predicted the maximum water volume fraction was obtained at 13:00 hr. i.e. 0.999998. The red line in the figure visualizes the vapor volume fraction while the blue line visualizes time on the streamline. As seen increment in the temperature, the volume fraction of vapors rises remarkably and air lessens remarkably.

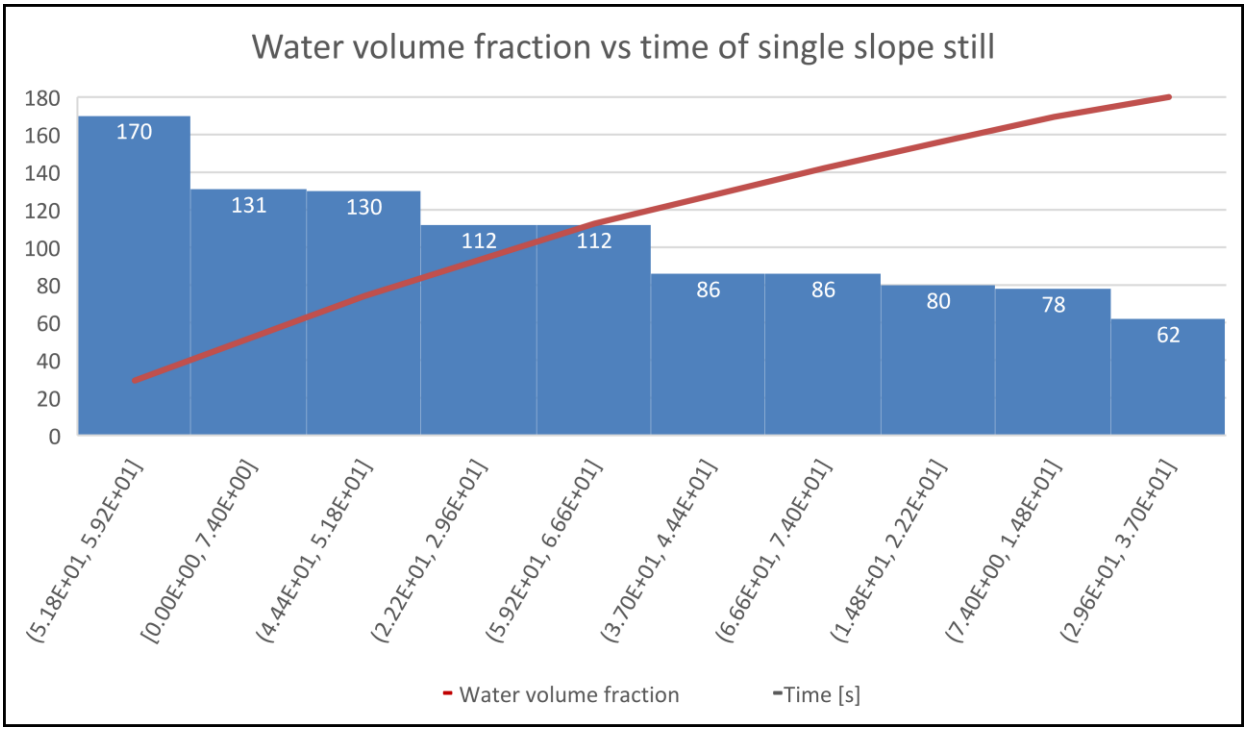

Fig 21. Water volume fraction concerning the time of single slope solar still.

Figure 22 visualizes the vapor volume fraction of single slope solar still concerning the time. The vapor volume fraction of the single-slope solar still is calculated for the entire day. From the simulation result, it was predicted the maximum vapor volume fraction was obtained at 13:00 hr. i.e. 0.999998. The red line in Figure 22 shows the water volume fraction while the blue line shows time on the streamline. From the graph of a single solar still, the conversion of water into vapor increases as time increases. It results in more conversion of water into vapor is obtained at 13:00 because of higher solar flux and after as time increases, vapor conversion decreases.

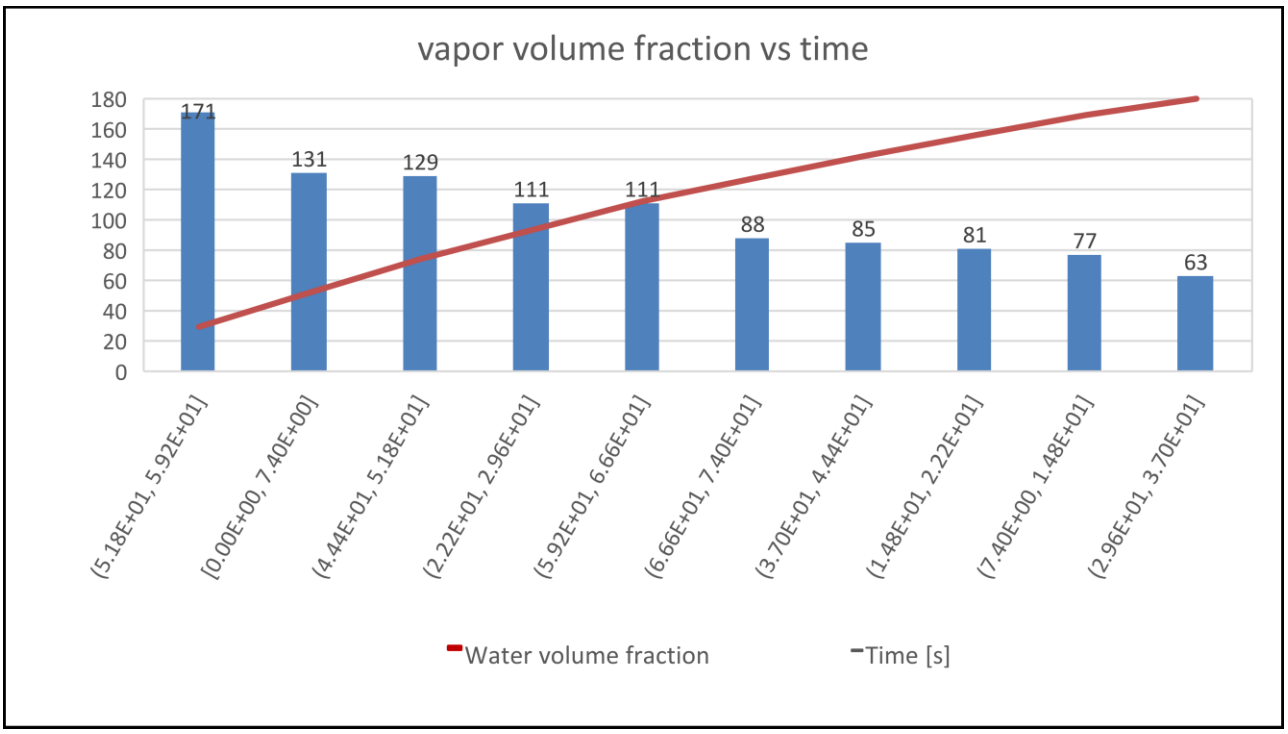

Fig 22. Vapor volume fraction concerning the time of single slope solar still.

Figure 23 visualizes the vapor volume fraction of the double slope solar still concerning the time. The vapor volume fraction of the double slope solar still is calculated for the entire day. From the simulation result, it was predicted the maximum vapor volume fraction was also obtained at the same time at 13:00 hr. i.e. 0.999999. The red line in figure 23 shows the water volume fraction while the blue line shows time on the streamline. First, vapor volume fraction increases with time, while after 14:20 hr. vapor volume fraction starts to decrease.

From the results of the vapor and water volume fraction of both solar stills, the maximum water volume fraction is of single slope solar still, whereas the maximum vapor volume fraction is of double slope solar still. And minimum water volume fraction occurred in double slope than single slope. So, the conversion of water into vapor occurred rapidly in a double slope than a single slope.

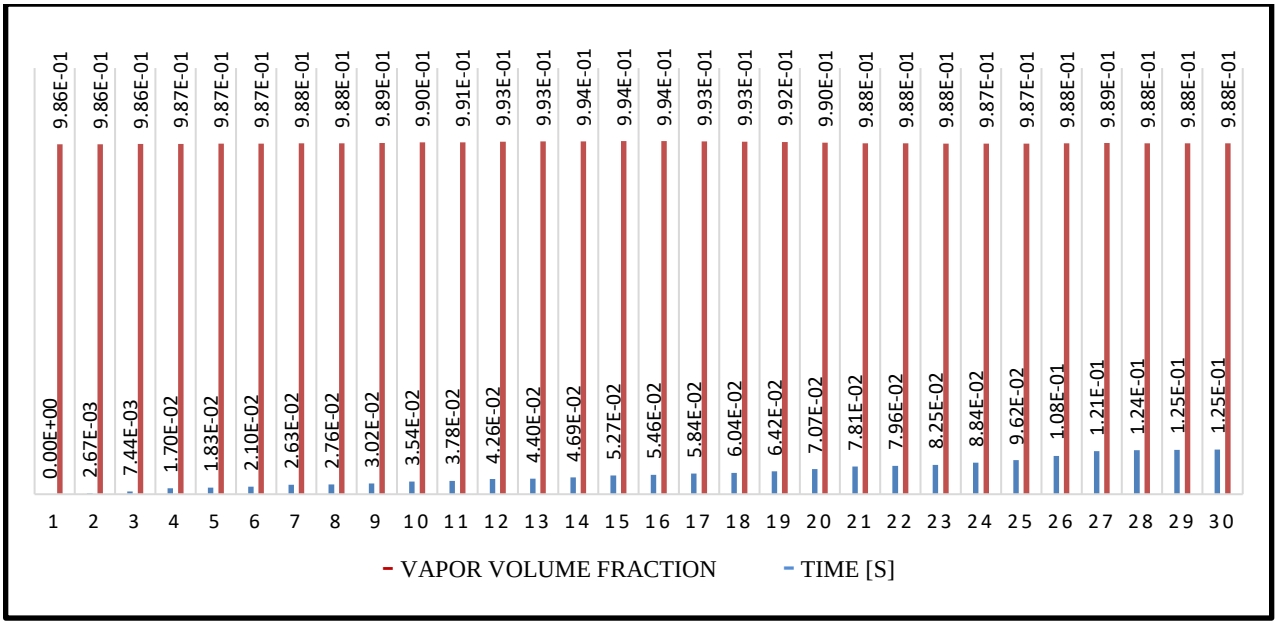

Fig 23. Vapor volume fraction concerning the time of double slope solar still.

4.5 PRESSURE VARIATION

Fig 17 and 18 respectively show the gas-phase pressure-volume rendering inside the single slope solar still and double slope solar still. Pressure variation at each stage was calculated inside the stills. In the pressure-volume rendering, the red color shows maximum pressure, while the blue color shows minimum pressure for both stills. The pressure inside a single solar still, firstly, increases, then decreases and again increases from top to bottom. The maximum pressure is calculated at the top while the minimum temperature is calculated at some height from the absorber. The minimum pressure inside the single slope still is approximately negligible. Pressure volume rendering shows the pressure near-transparent material is -4.8577 Pa while near opaque material, the pressure is 10.9478 Pa.

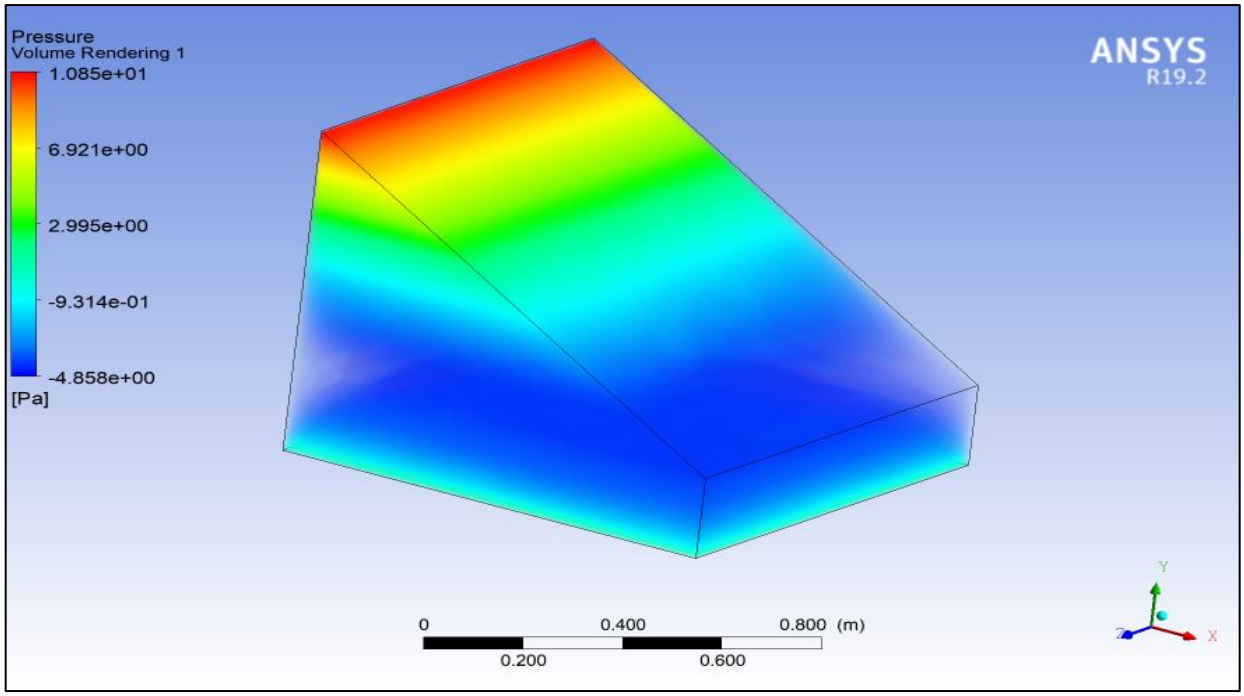

Fig 24. Pressure volume rendering inside the single slope solar still.

Figure 25 visualizes pressure, inside double slope solar still, which is approximately constant. The maximum pressure is calculated near corners on both sides, while minimum temperature is calculated everywhere except corners. The minimum pressure inside the double slope still is approximately negligible. Pressure volume rendering shows the pressure near-transparent material is -583.058 Pa while near opaque material, the pressure is 2028.78 Pa. From the pressure-volume rendering of both stills, it has been observed that pressure in double slope still is more contrast to single slope still.

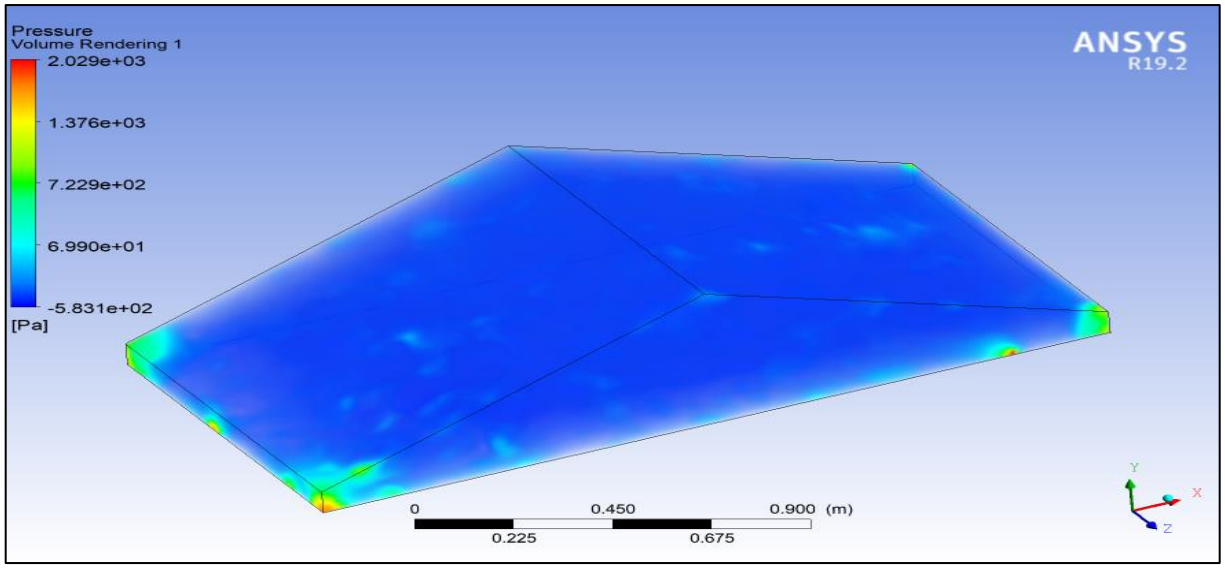

Fig 25. Pressure volume rendering inside the double slope solar still.

Figure 26 visualizes the pressure variation of single slope solar still concerning the time. The pressure of the single-slope solar still is calculated for the entire day. From the simulation result, it was predicted the maximum pressure was obtained at 13:00 hr. i.e. 10.9478 Pa. The red line in the graph shows the pressure variation while the blue line shows time on the streamline. With increase time, the pressure of the mixture changes slightly and maximum pressure occurred near opaque material.

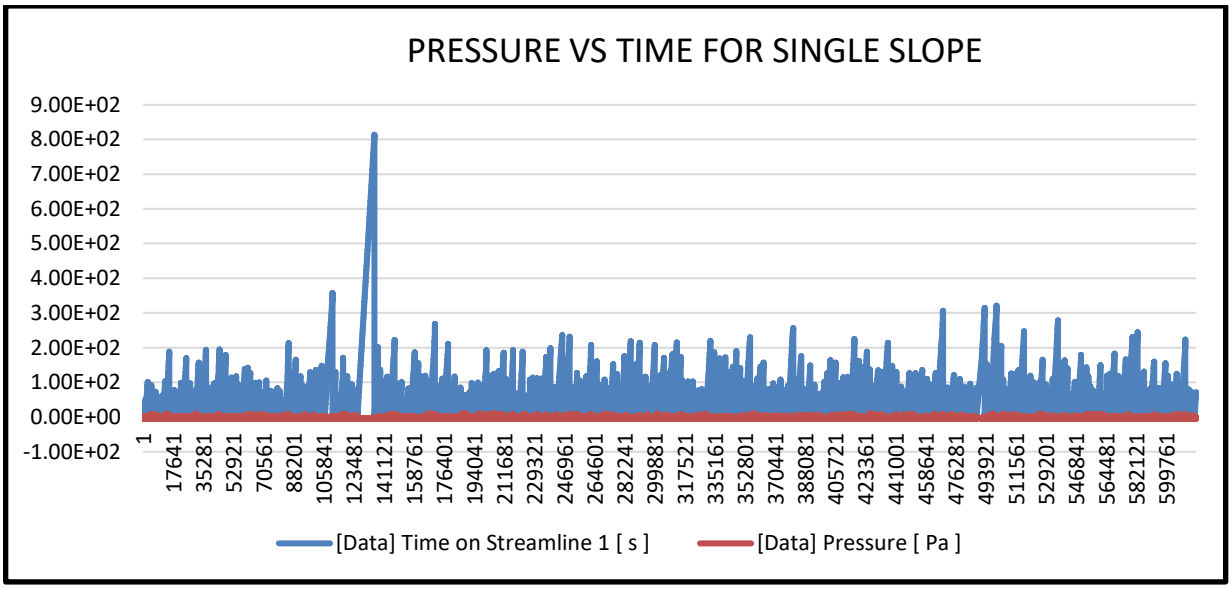

Fig 26. Pressure variation concerning time inside single slope solar still.

Figure 27 shows the pressure variation of the double slope solar still concerning the time. The pressure of the single-slope solar still is calculated for the entire day. From the simulation result, it was predicted the maximum pressure was obtained at 13:10 hr. i.e. 2028.78 Pa. The red line in figure 27 shows the pressure variation while the blue line shows time on the streamline. With increase the time, the pressure of the mixture changes very highly near opaque material compared to single slope still and near-transparent material, pressure remains almost constant which is very less. Maximum pressure occurred near opaque material which is higher than single slope still. In a comparison of both stills, it has been observed that double slope solar still has higher pressure variation with time than single slope solar still.

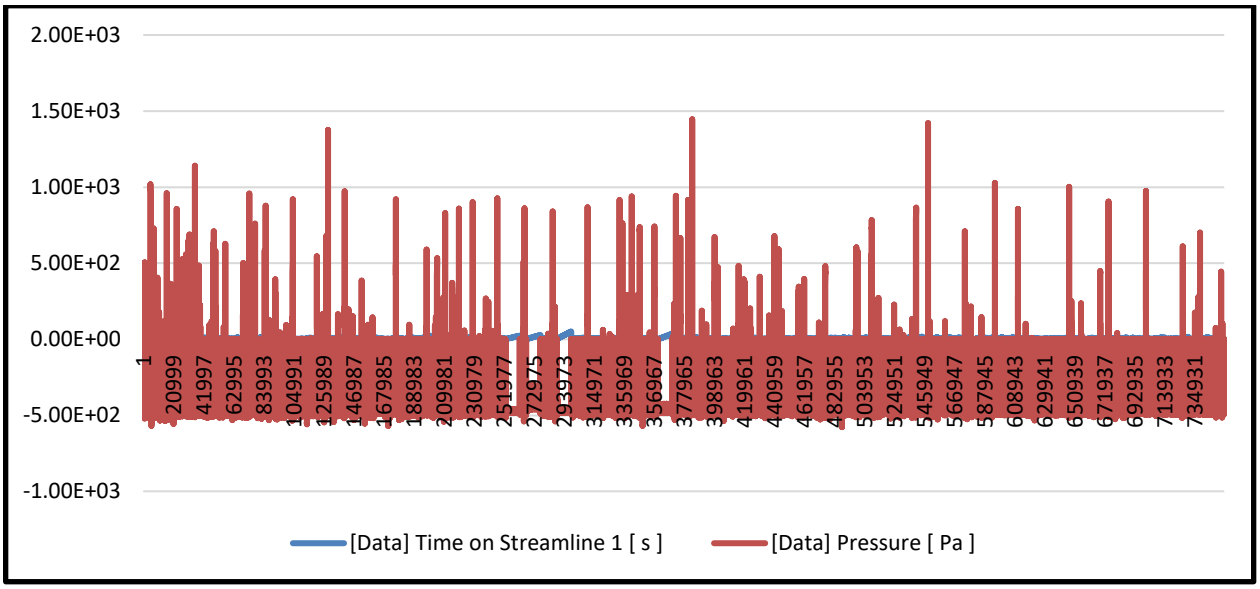

Fig 27. Pressure variation concerning time inside double slope solar still.

4.6 VELOCITY DISTRIBUTION

Figure 28 shows the velocity volume rendering of the mixture inside the single slope solar still. The minimum velocity of the mixture is near-transparent material which is zero while the highest value of the velocity is near opaque material i.e. 0.789541ms^{-1}.

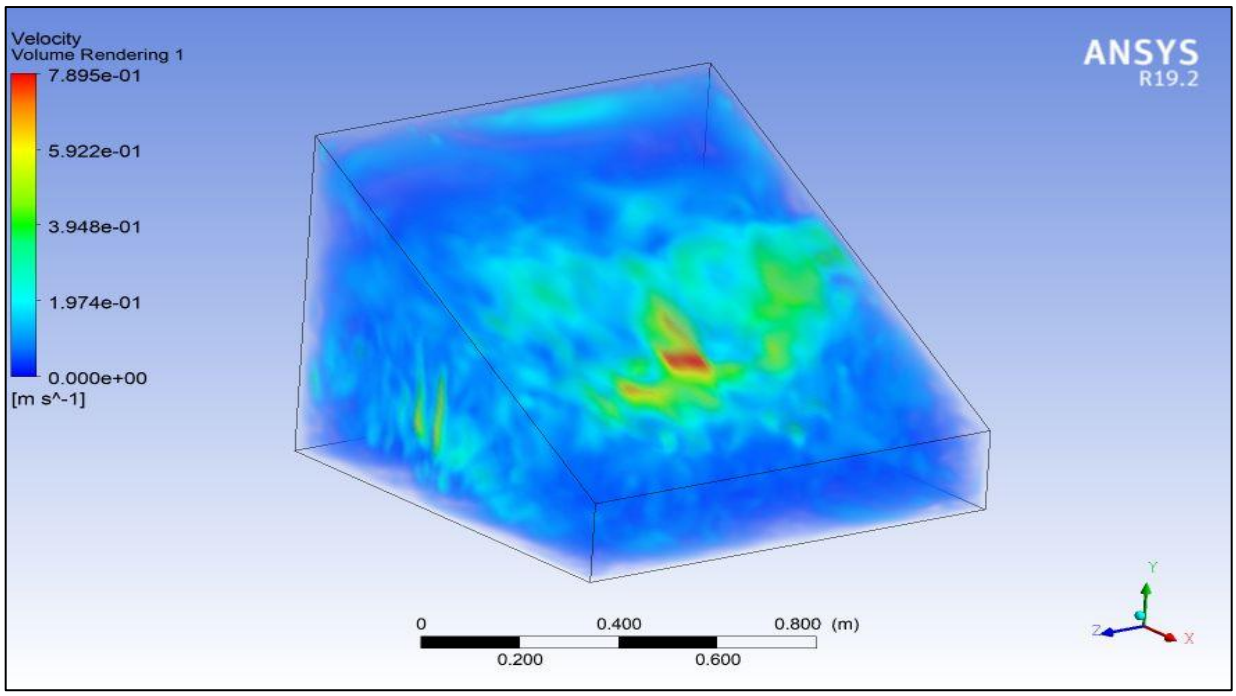

Fig 28. Velocity volume rendering inside the single slope solar still.

Figure 29 visualizes the velocity volume rendering of the mixture inside the double slope solar still. The minimum velocity of the mixture is near-transparent material which is zero while the maximum velocity is near opaque material i.e. 11.8199 ms^{-1}. In volume rendering, the red color visualizes high velocity whereas blue color visualizes less velocity. In volume rendering, the color is changing from blue to red. The red color in the double slope is showing only near the glass surface.

The comparison of both stills for velocity distribution, it has been noticed that the velocity of the mixture is more in double slope than single slope solar still. More velocity shows more circulation of mixture particle inside the still i.e., conversion of water into vapor and moves upward to produce potable water

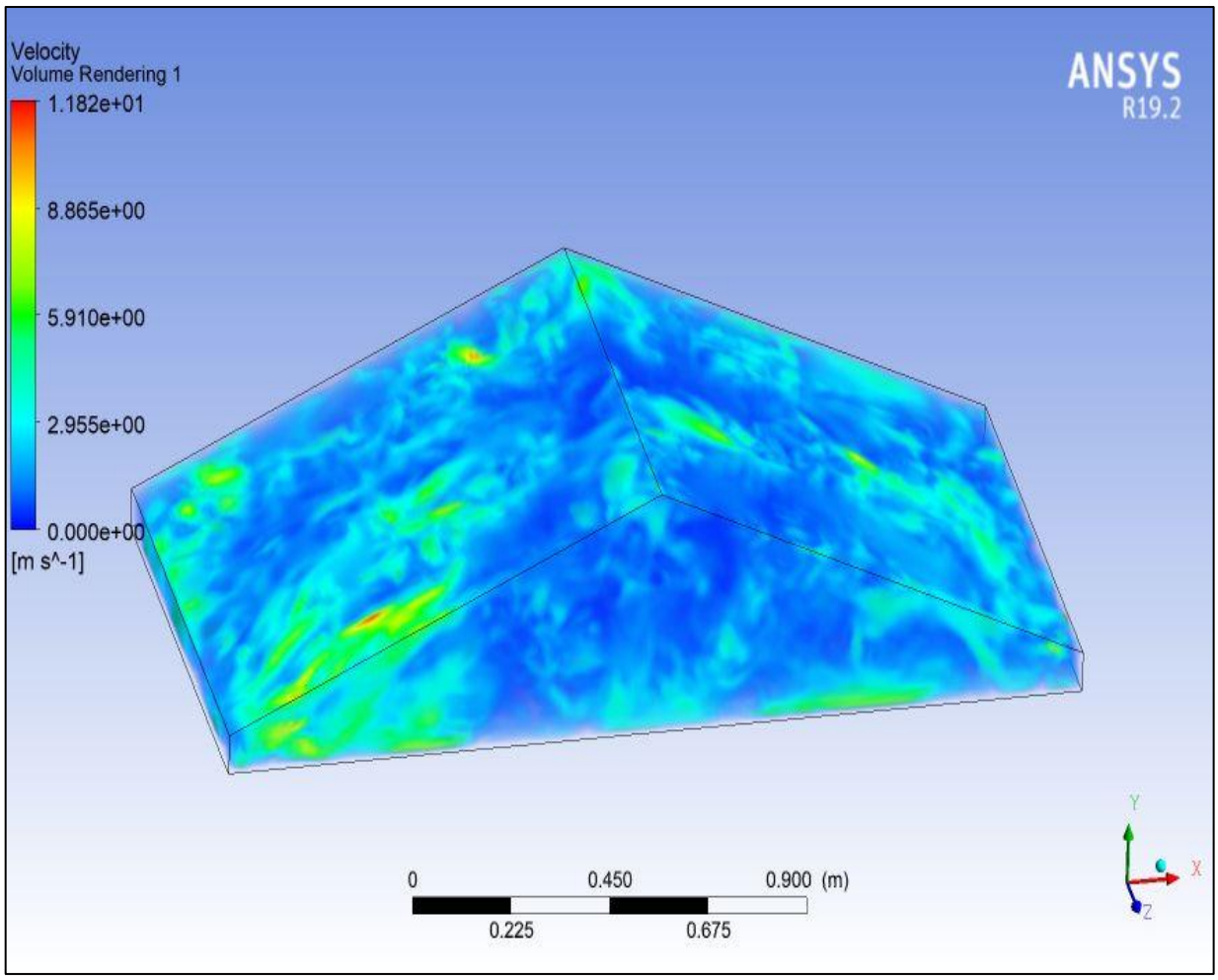

Fig 29. Velocity volume rendering inside the double slope solar still.

4.7 MASS FLOW

Figure 30 visualizes the mass flow rate inside the single slope solar still. In mass flow contour, the red color shows a high mass flow rate while blue color shows low mass flow inside the single slope solar still. Inside the still, different colors are distributed to calculate the mass flow rate at each stage.

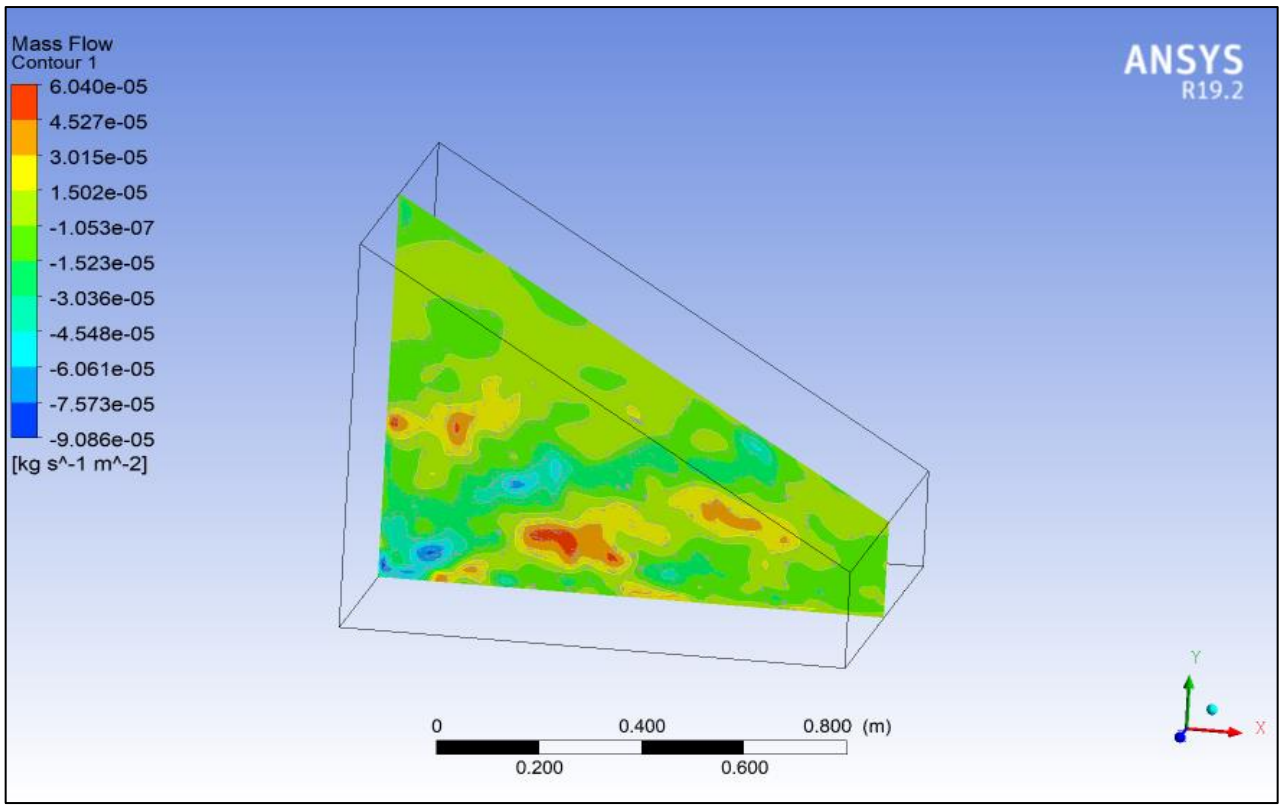

Fig 30. Mass flow contour inside the double slope solar still.

Figure 31 visualizes the mass flow rate inside the double slope solar still. In mass flow contour, the red color shows a high value of mass flow rate while the blue color shows a low value of mass flow inside the double slope solar still. Inside the still, different colors are distributed to calculate the mass flow rate at each stage. Mostly inside the solar still, the yellow color is seen which shows the range of mass flow from -3.763e-04 to 3.114e-03 $kgs^{-1}m^{-2}$.

The comparison of both stills for mass flow rate shows that the mass flow rate is finer inside double slope solar still than single slope solar still. The maximum mass flow in single slope is 6.05e-05 $kgs^{-1}m^{-2}$ while in double slope, maximum mass flow is 1.009e-02 $kgs^{-1}m^{-2}$.

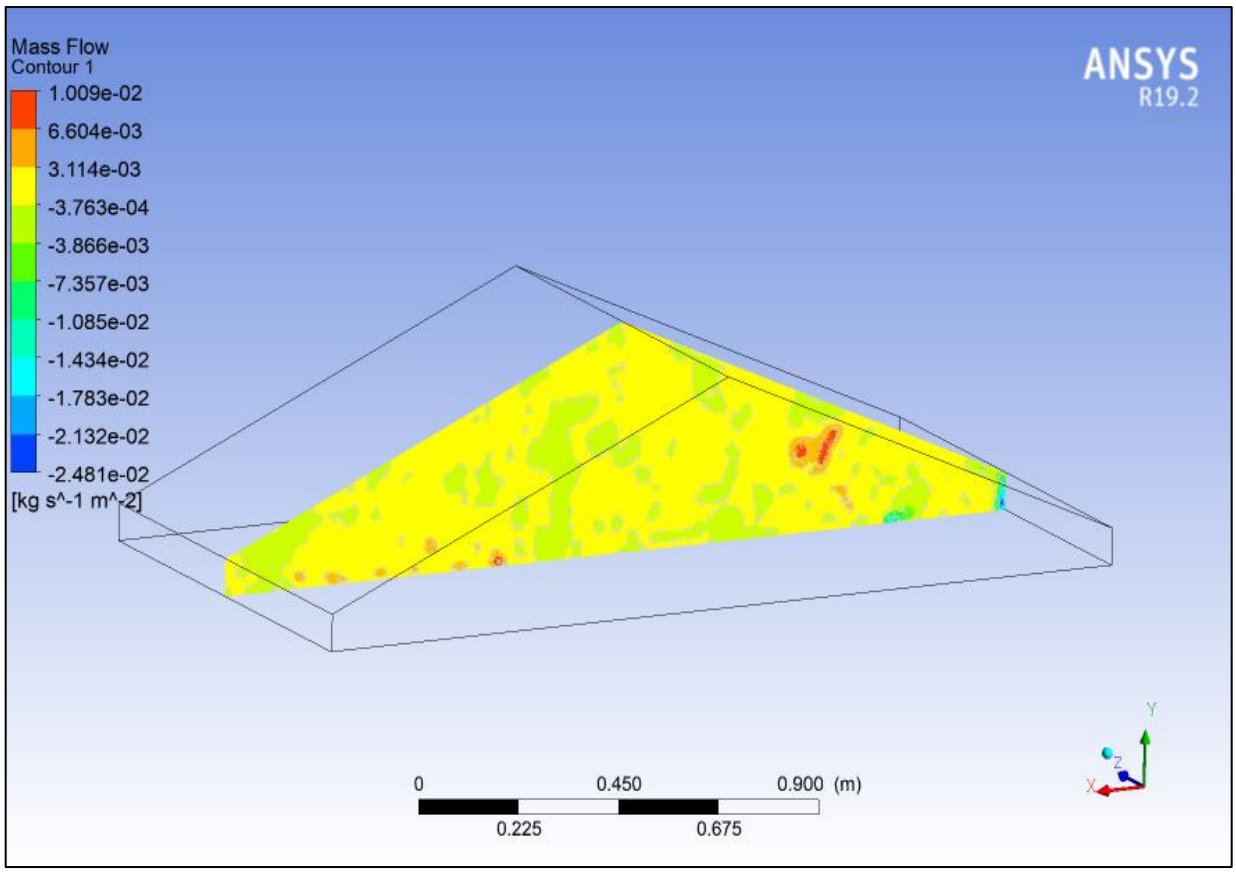

Fig 31. Mass flow contour inside the double slope solar still.

4.8 STATIC ENTHALPY

Figure 32 shows the static enthalpy inside the single slope solar still. In static enthalpy volume rendering, the red color visualizes the maximum value of static enthalpy while the blue color visualizes the minimum value of static enthalpy inside the single slope solar still. Inside the still, different colors are distributed to calculate static enthalpy at each stage. The minimum static enthalpy of the mixture is near-transparent material which is -1.62801e+07 Jkg^{-1} while maximum static enthalpy is near opaque material i.e. -1.11587e+07 Jkg^{-1}. The negative value of static enthalpy means energy is absorbed by water to convert into vapor. In single slope solar still, the static enthalpy is increasing from bottom to top rapidly whereas in double slope solar still, the temperature is increasing slowly from bottom to top. Both stills are attaining maximum static enthalpy at the top because of the orientation of mesh towards solar incident rays.

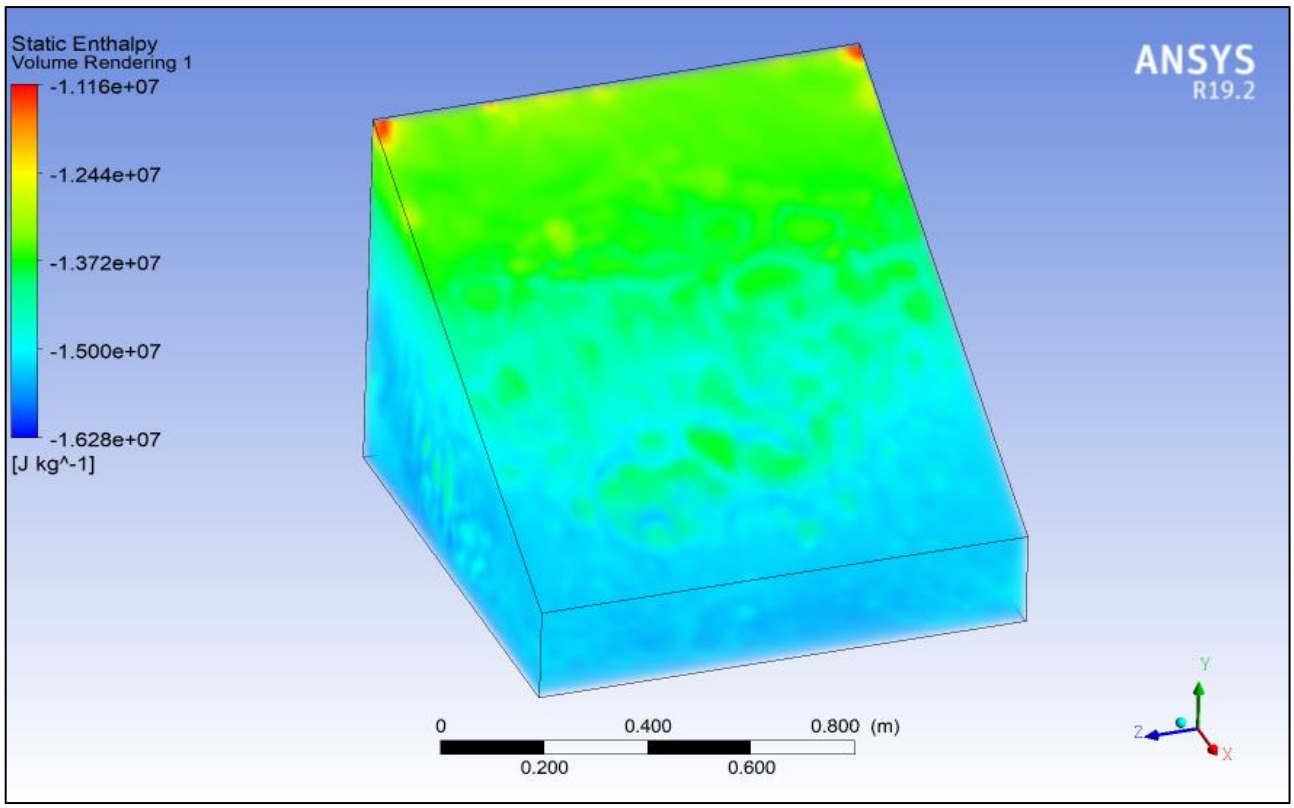

Fig 32. Static enthalpy volume rendering inside the double slope solar still.

Figure 33 shows the static enthalpy inside the double slope solar still. In static enthalpy volume rendering, the red color visualizes the maximum value of static enthalpy while the blue color visualizes the lowest value of static enthalpy inside the single slope solar still. Inside the still, different colors are distributed to calculate static enthalpy at each stage. The minimum static enthalpy of the mixture is near-transparent material, which is -1.690531e+07 Jkg^{-1} while maximum static enthalpy is near opaque material i.e., 1.06879e+07 Jkg^{-1}. The negative value of static enthalpy means energy is absorbed by water to convert into vapor.

The comparison of both stills shows static enthalpy absorbed by double slope solar still is better contrast to single slope solar still, which affects the production of potable water. More absorption of enthalpy from sunlight shows more conversion of water molecules into vapor, at 13:10 hr maximum enthalpy absorbed by single slope while in double slope solar still, maximum enthalpy is absorbed in 13:30 hr. This difference is because of mesh orientation difference and also depends on glass size.

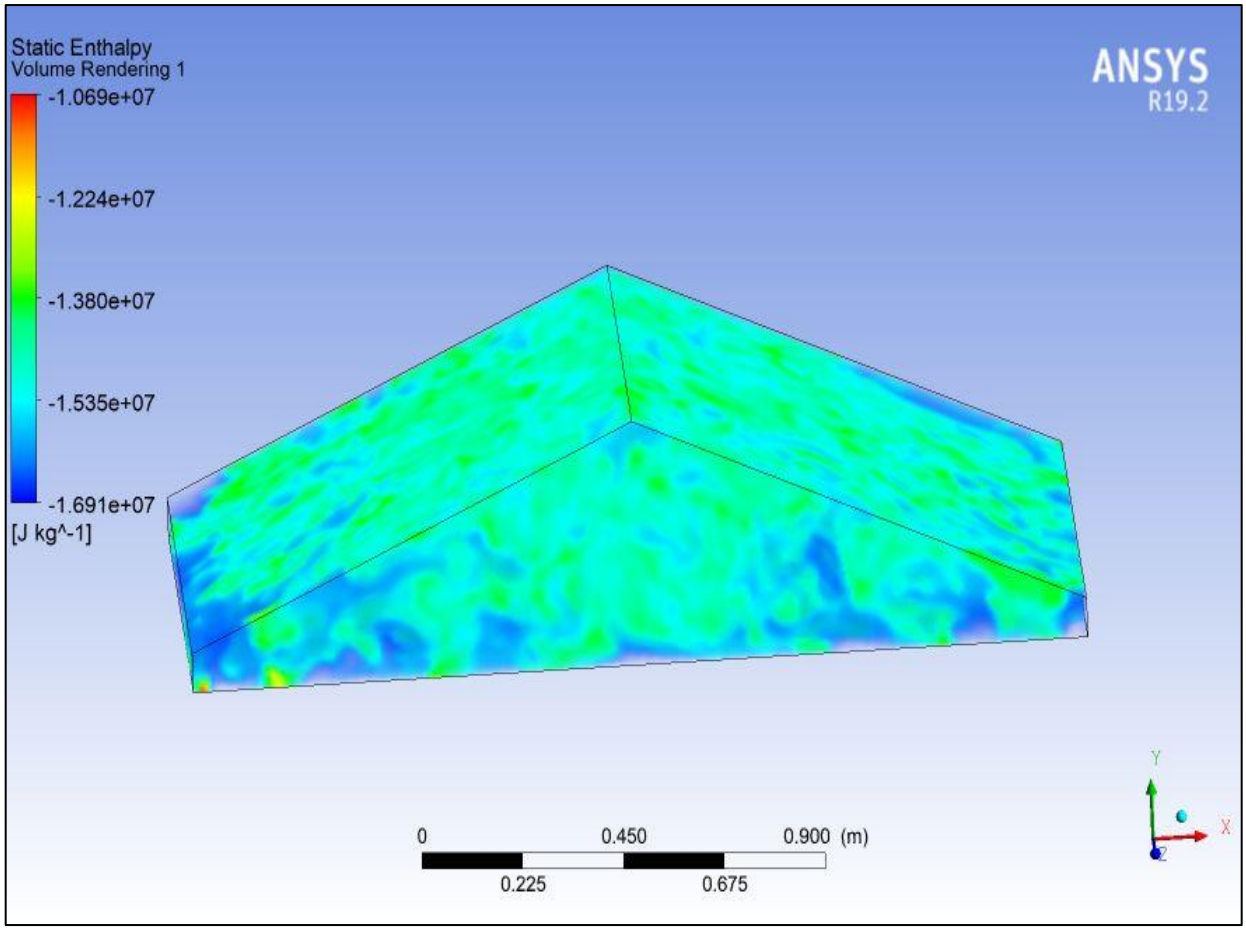

Fig 33. Static enthalpy volume rendering inside the double slope solar still.

4.9 ABSORPTION COEFFICIENT

The absorption coefficient relates to the intensity attenuation of the light passing through a material. Figure 34 shows the absorption coefficient volume rendering in which blue color visualizes the lowest value and red color visualizes the highest value of the absorption coefficient. Inside the single slope solar still, the red color is more compared to other colors which mean higher solar energy is taken up by the glass and then, transmitted through the glass into the still. The maximum value of the absorption coefficient is 0.539999 m^{-1} near opaque material while the lowest value of the absorption coefficient is 0.470670 m^{-1} near-transparent material inside still. The lowest value of the absorption coefficient on glass is at both upward corners and in the middle part and downward corners of the glass, the absorption coefficient is higher.

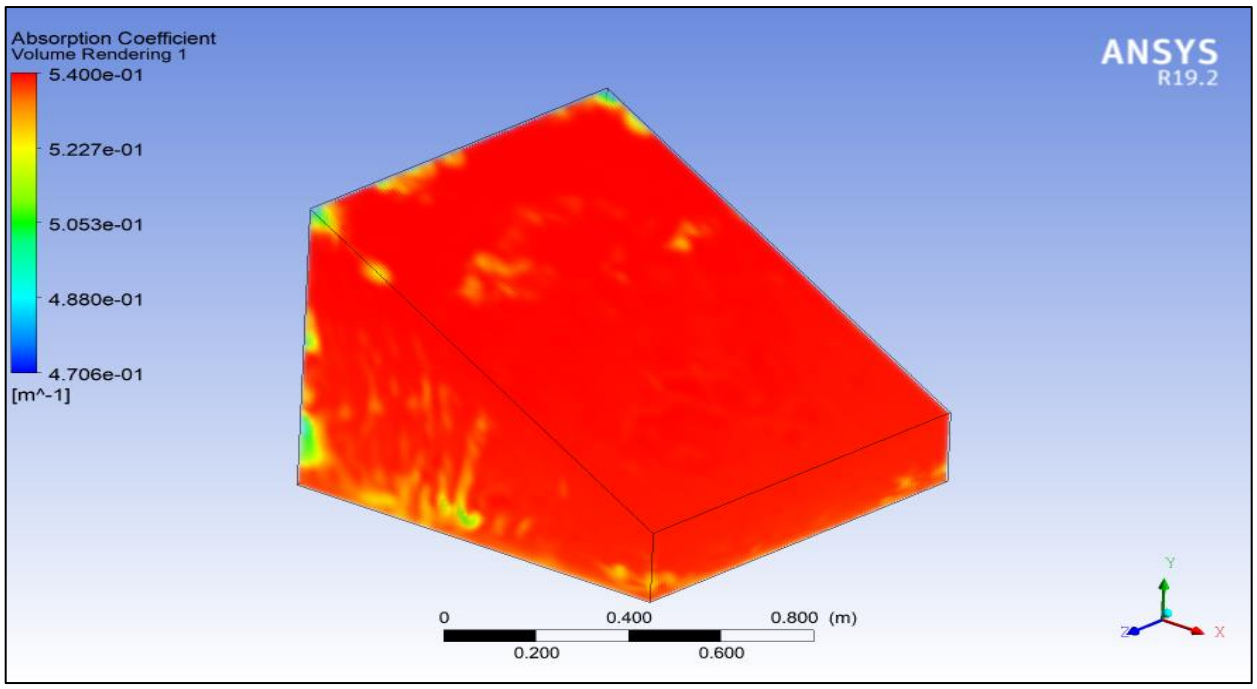

Fig 34. Absorption coefficient volume rendering inside the single slope solar still.

Figure 35 visualizes the absorption coefficient volume rendering of double slope solar still in which blue color visualize the lowest value and red color visualize the highest value of the absorption coefficient. Inside the single slope solar still, the red color is more compared to other colors which mean higher solar energy is taken up by the glass and then, transmitted through the glass into the still. The maximum value of the absorption coefficient is 0.54 m^{-1} near opaque material while the lowest value of the absorption coefficient is 0.000495335 m^{-1} near-transparent material inside still. The lowest value of the absorption coefficient on glass is at both upward corners and in the middle part and downward corners of the glass, the absorption coefficient is higher.

In the comparison of the absorption coefficient of both stills, it has been noticed about the absorption coefficient of the double slope is more compared to single slope because of the size of the glass of double slope solar still. Solar energy is absorbed by double slope is higher in contrast with single slope solar still. From the temperature distribution result, it was calculated that double slope solar still has less temperature in contrast with single slope but the pressure and heat absorption are higher of double slope solar still which affects the production of potable water.

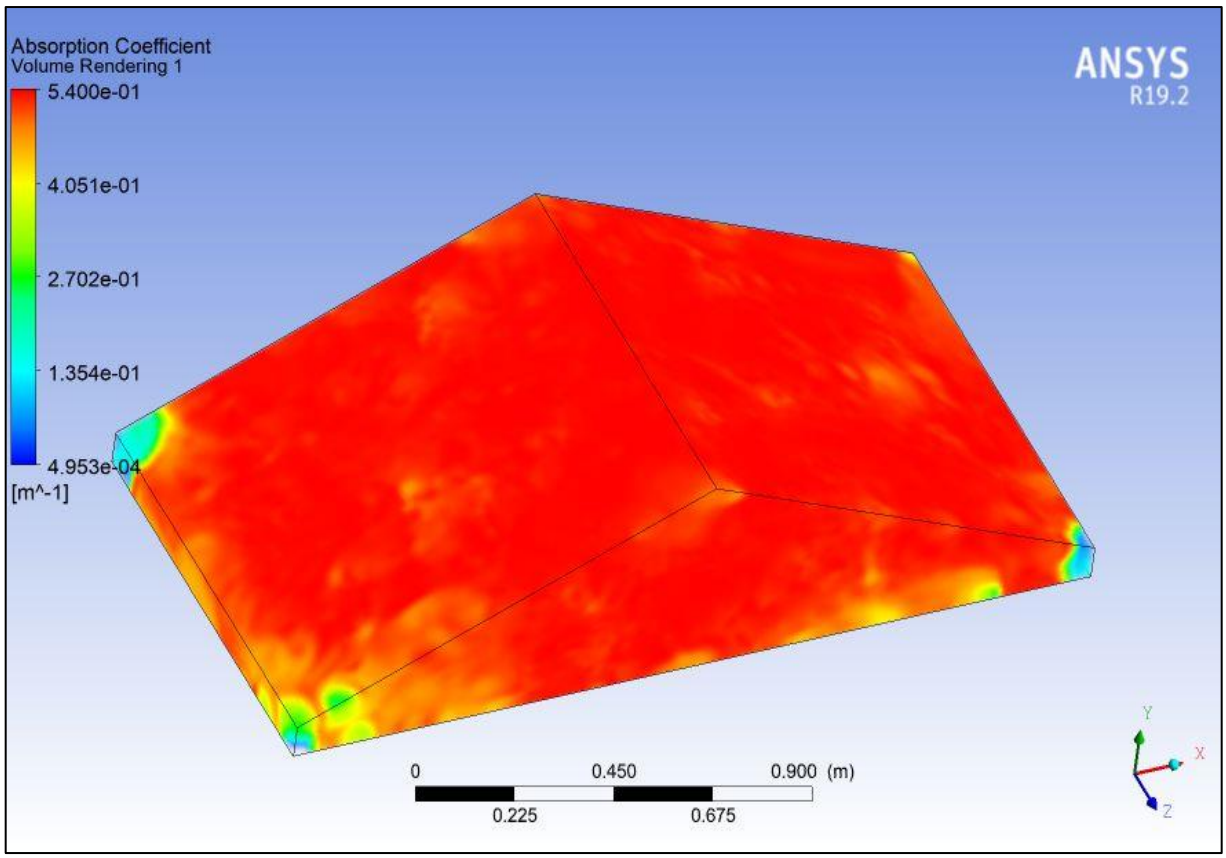

Fig 35. Absorption coefficient volume rendering inside the double slope solar still.

4.10 DO IRRADIATION

Figure 36(a) and 36(b) show do irradiation volume rendering inside the single slope and double slope solar still. Red color visualizes maximum irradiation while blue color visualizes minimum irradiation. From both stills volume rendering, it is calculated that single slope has maximum irradiation 1294.8 Wm^{-2} and a minimum 10.8502 Wm^{-2}, in double slope solar still maximum irradiation is calculated 7.32235 Wm^{-2} and minimum 0.587949 Wm^{-2}.

Single slope solar still has higher irradiation contrast to double slope solar still. Irradiation is the process by which still is disclosed to radiation. The Exposure of solar rays is more towards single slope still in contrast with double slope solar still. More irradiation means more temperature generation inside the still, which is only inside single slope solar still.

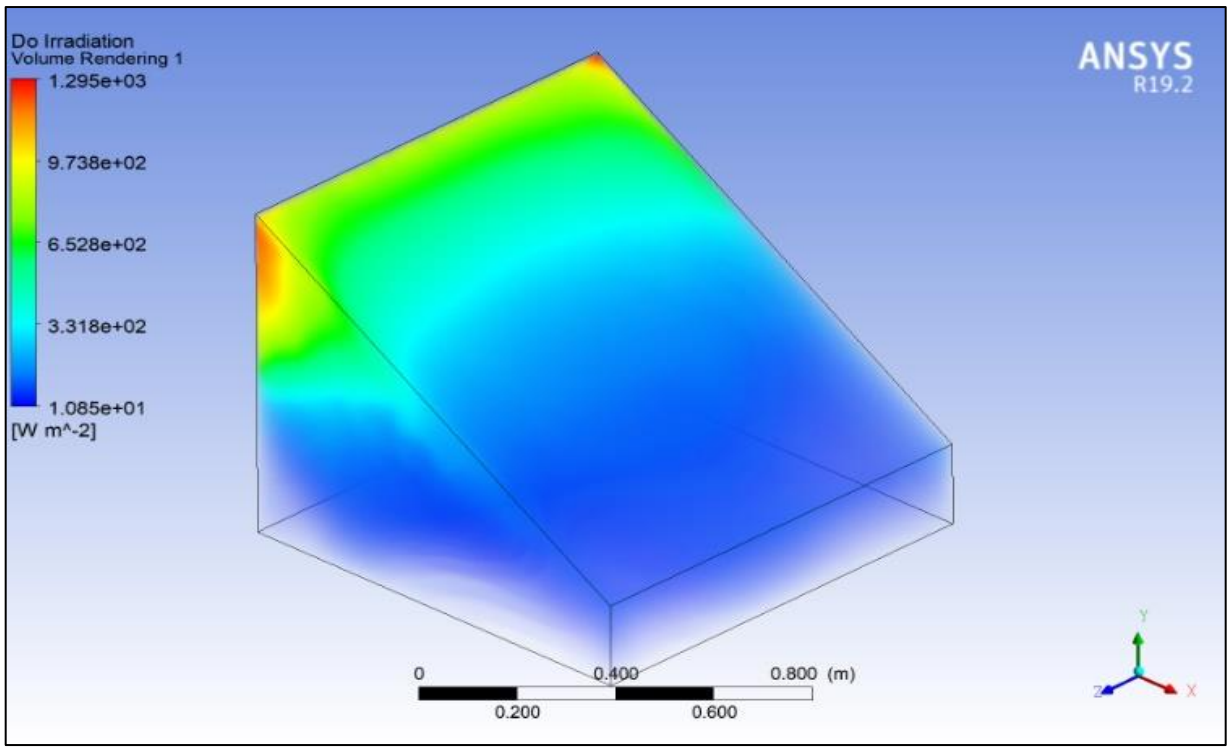

Fig 36(a). Do irradiation volume rendering inside the single slope solar still.

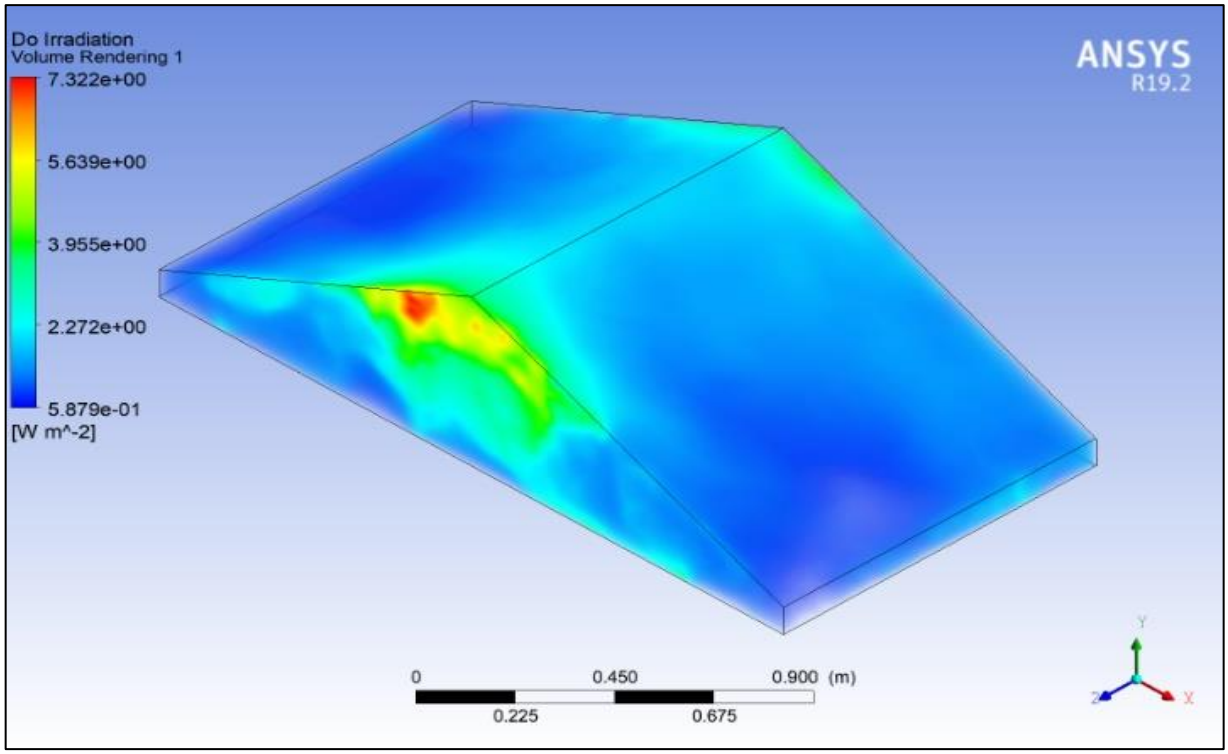

Fig 36(b). Do irradiance volume rendering inside the double slope solar still.

4.11 EDDY VISCOSITY

Figure 37 shows the eddy viscosity of the mixture inside the single slope solar still. The red color in legend shows maximum eddy viscosity while blue color shows minimum eddy viscosity. The maximum eddy viscosity in single slope solar still is 0.0439431 Pa s and minimum eddy viscosity is 2.15024e-05 Pa s. At the corners of still, eddy viscosity is zero.

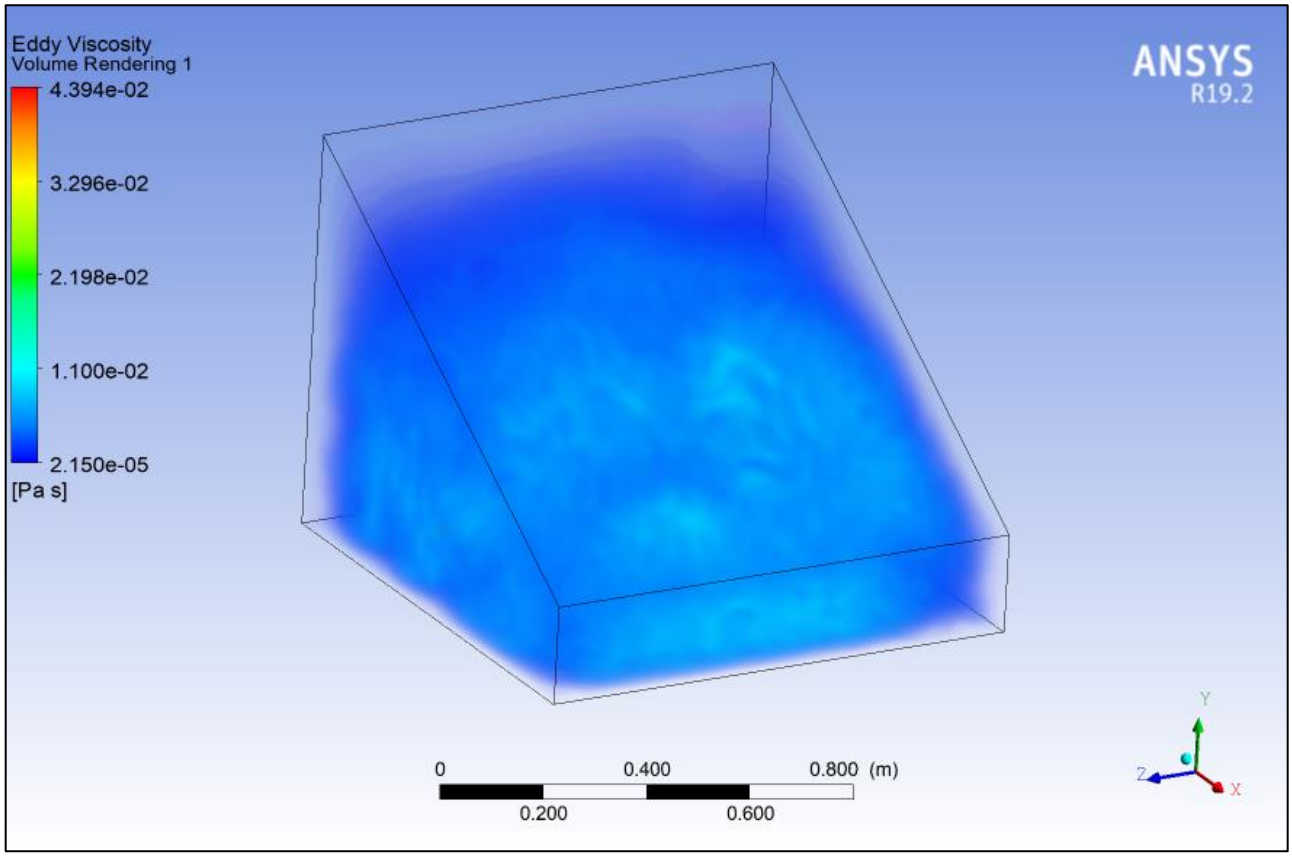

Fig 37. Eddy viscosity volume rendering inside the single slope solar still.

Figure 38 visualizes the eddy viscosity of the mixture inside the single-slope solar still.

The red color in legend shows maximum eddy viscosity while blue color shows minimum eddy viscosity. The maximum eddy viscosity in still is 0.596871 Pa s and minimum eddy viscosity is 0.000975535 Pa s.

Eddy viscosity is a proportionality factor that describes turbulent transfer energy in the form of moving eddies. Higher eddy viscosity is calculated inside the double slope than single slope. Hence, turbulence is higher in double slope due to which mixture circulates

more inside double slope than single slope and particles of the mixture strike on the walls, which results in pressure increase inside the double slope solar still.

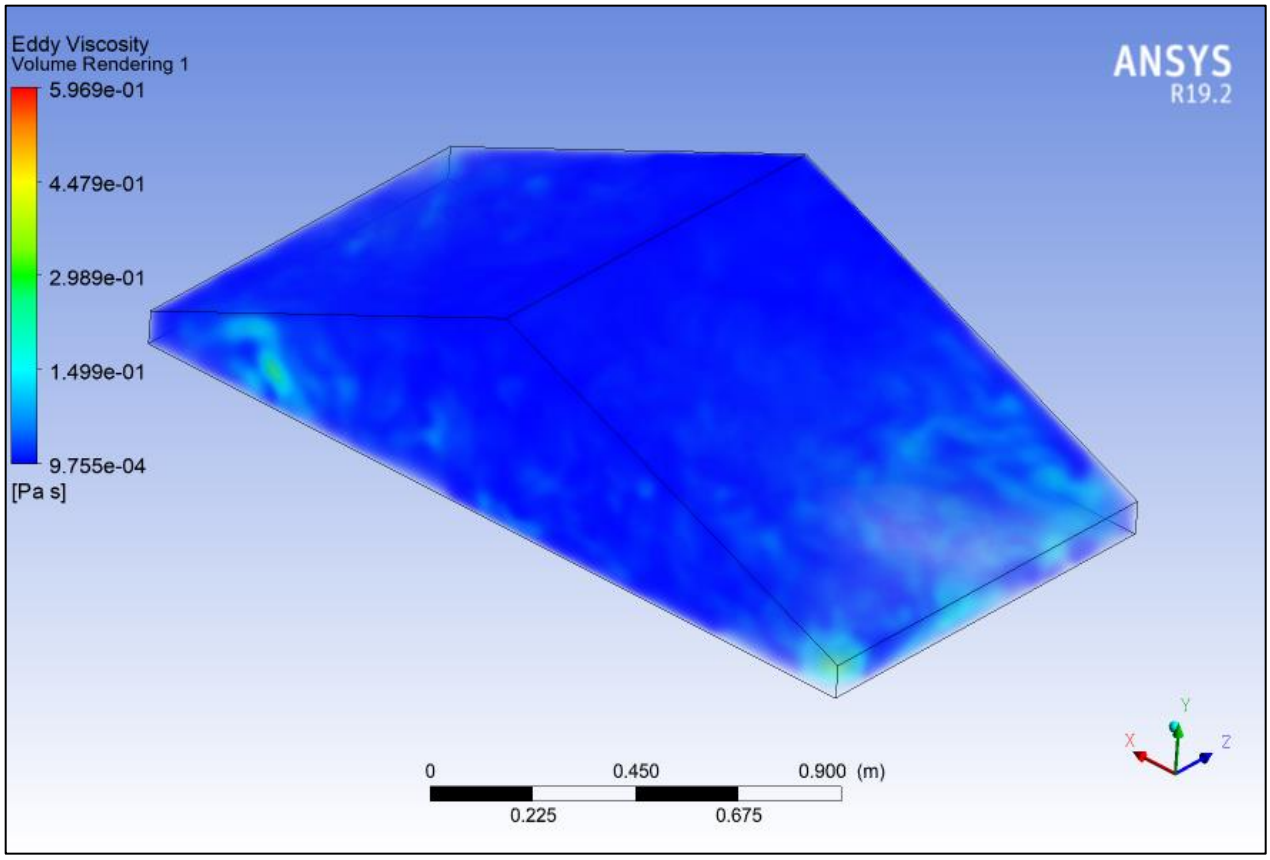

Fig 38. Eddy viscosity volume rendering inside the double slope solar still.

4.12 SOLAR HEAT FLUX

Figure 39 shows the solar heat flux variation of single slope solar still concerning the time. The solar heat flux of the single-slope solar still is calculated for the entire day. The Red line in Figure 39 shows solar heat flux while the blue line shows the time of streamline. From the simulation result, it was predicted the solar heat flux first raises with time after sunrise and then starts to lessen as time increases afternoon. The maximum solar flux was obtained at 13:00 hr. due to which still gains high temperature while the minimum solar heat flux was obtained in the morning during sunrise and sunset which produce low temperatures to convert the water into vapor. Solar heat flux again slightly increases after 14:30 hr. and then again decrease. After 15:15 hr. solar heat flux increases

but not for more time. This process continues until sunset. From the graph of a single solar still, it is also predicted that there is no time when the solar heat flux inside the single solar still is constant.

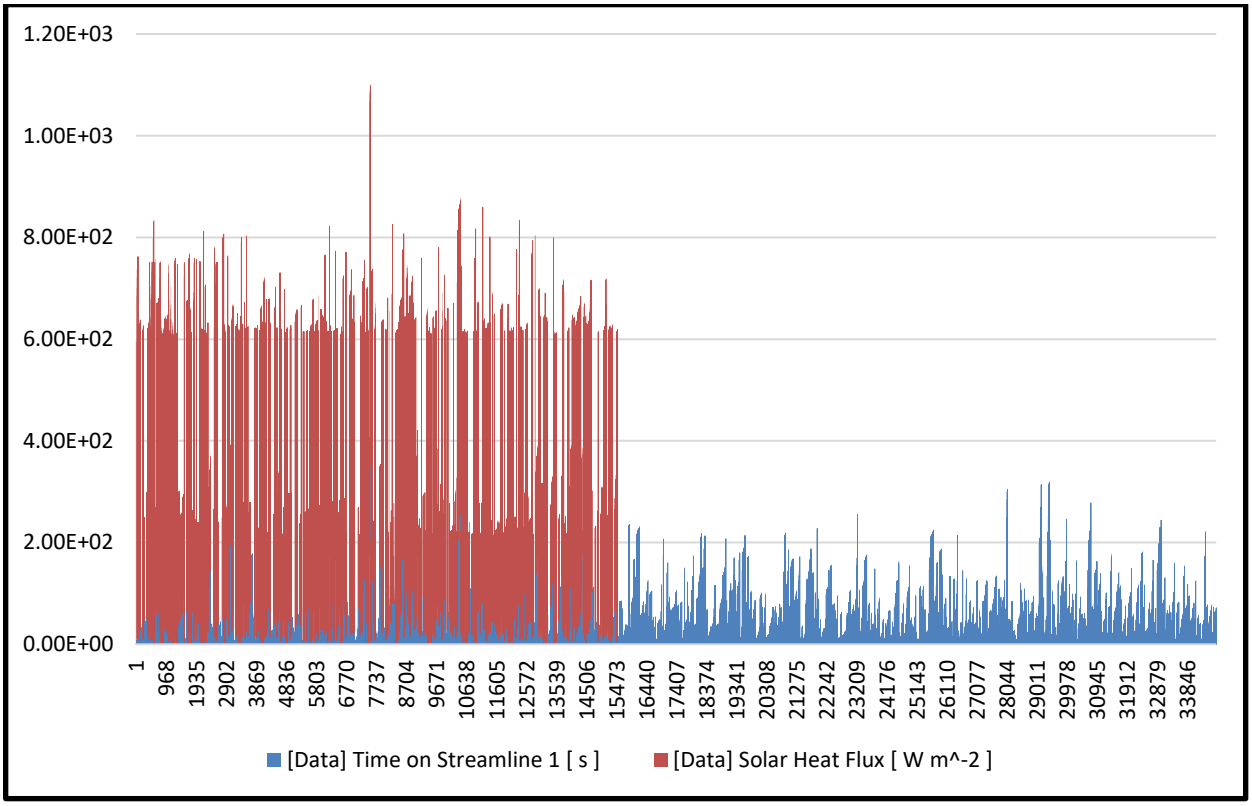

Fig 39. Solar heat flux concerning time inside the single slope solar still.

Figure 40 shows the solar heat flux variation of single slope solar still concerning the time. The solar heat flux of the double slope solar still is calculated for the entire day. The red line in figure 40 shows solar heat flux while the blue line shows the time of streamline. From the simulation result, it was predicted the solar heat flux remains almost constant with time after sunrise. The maximum solar flux was obtained at 12:30 hr due to which still gains high temperature while the minimum solar heat flux was obtained in the morning same as during sunrise and sunset which produce low temperature to convert the water into vapor. Solar heat flux remains almost constant from 10:00 hr. to 14:00 hr. This action proceeds until the sunset. In the evening, solar heat flux becomes negligible.

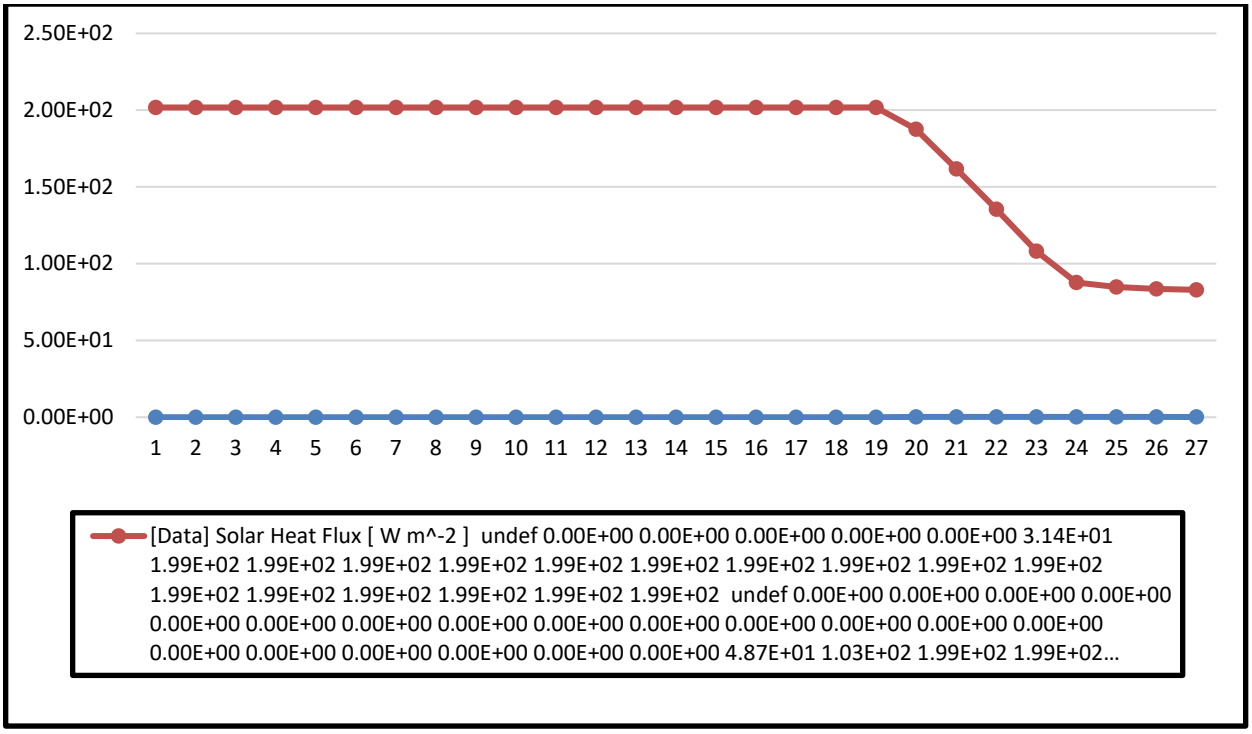

Fig 40. Solar heat flux concerning time inside the double slope solar still.

4.13 WATER PRODUCTION RATE

Figure 41 visualizes the graph of the rate of the production of the water concerning the time. The simulation of single slope solar still runs in 5 hr. time. In this figure, it is noted that as the action starts at 8:00 hr., time passes and water starts to warm up due to solar radiation absorbed by water. Moderately still space heats up with water vapor and the freshwater production rate raises till 13:00 hr. and later when solar radiation decreases water moves downward slowly.

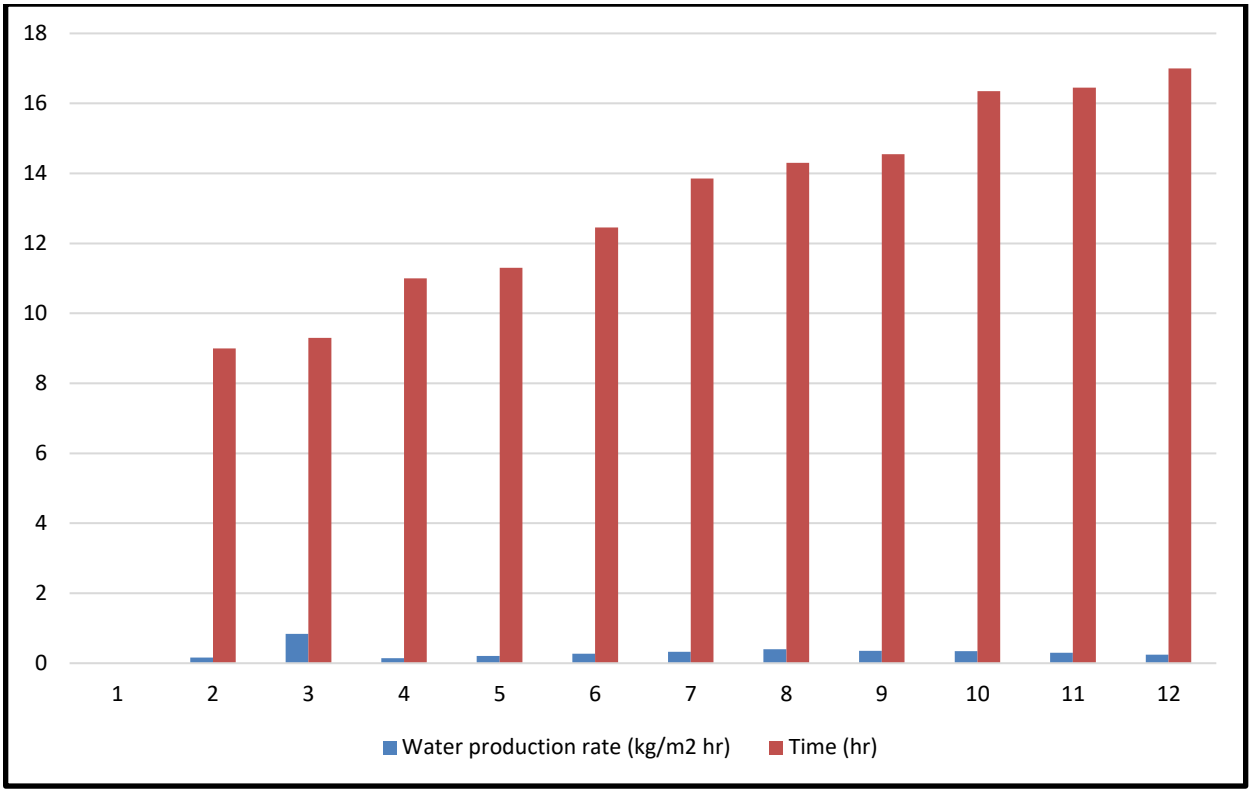

Fig 41. Water production rate concerning time inside the single slope solar still.

Figure 42 visualizes the graph of the water production rate concerning the time. The simulation of double slope solar still runs at 6.30 hr. time. In this figure, it is noted that as the action starts at 8:00 hr., time passes and water starts to warm up due to solar radiation absorbed by water. Moderately still space heats up with water vapor and the freshwater production rate raises till 13:30 hr and after when solar radiation decreases water moves to downward slowly.

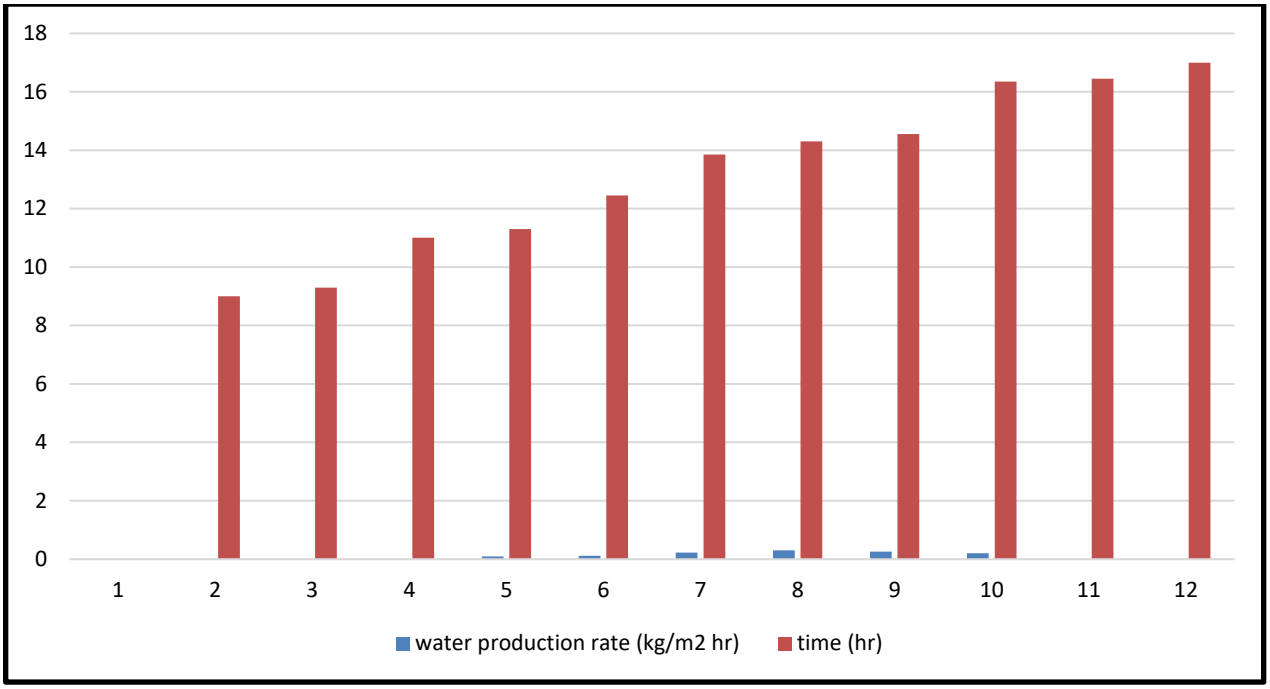

Fig 42. Water production rate concerning time inside the double slope solar still.

In a comparison of water production of both stills, it was observed that water production of single slope is more compared to double slope solar still. Some terms affect water production, such as temperature, mass flow, pressure, solar heat flux, absorption coefficient, and many other factors. These all terms are checked in the simulation of both stills and observed that a single slope is more capable of producing freshwater in rural and urban areas both.

CHAPTER 5

CONCLUSION

The major motive of the research is to make a computational fluid dynamics model of single-slope and double-slope solar still. Two different two-phase three-dimensional models using computational fluid dynamics have been developed. In both stills, evaporation and condensation processes take place. The models were organized for water-mixture (air and water vapor) systems with the purpose of ANSYS FLUENT V19.2 software. The computational fluid dynamics simulation was conducted for transient conditions using these models. The simulation data of both systems were obtained in 5 hours and 6.30 hours with 10 steps of 15 minutes period. In both systems, water absorbs solar radiation and evaporates and the vapor condenses on the glass.

The main conclusions of the study are:

- The maximum temperature of air and water-vapor mixture inside the single slope is 435.399 K and the minimum temperature is 22.283 K
- The maximum temperature of the mixture inside the double slope is 92.1204 K and the minimum temperature is 25.6081 K
- It was found that the temperature remains almost constant from 13:00 to 13:30 in double slope. Then, it again shows the variation while single slope solar still continuously variates.
- The minimum temperature of the double slope is more compared to the single-slope solar still.
- The maximum volume fraction is near absorber i.e 0.0183968 and a minimum 1.8773×10^{-6} in single slope and the maximum volume fraction inside the double slope is 0.225132 and a minimum 1.8773×10^{-6}.
- The maximum volume fraction of vapor is 0.999998 and a minimum of 0.871514 in single slope and maximum vapor volume fraction in double slope is 0.999999 and the minimum is 0.000917328.

- The pressure near-transparent material is -4.8577 Pa while near opaque material, the pressure is 10.9478 Pa in single slope and the pressure near-transparent material is -583.058 Pa while near opaque material, the pressure is 2028.78 Pa in double slope.
- The maximum mass flow in single slope is 6.05e-05 $kgs^{-1}m^{-2}$ while in double slope, maximum mass flow is 1.009e-02 $kgs^{-1}m^{-2}$.
- The maximum water production rate in a single slope is 0.84 kg $m^{-2}hr^{-1}$ while the maximum water production rate in the double slope is 0.26 kg $m^{-2}hr^{-1}$.

It was predicted that computational fluid dynamics results visualize that computational fluid dynamics are strong equipment for the designing process, variable investigation, and can be used for removing difficulties during geometry creating of solar still construction. In the future, further work can be done by modifying different design parameters and orientation of solar still

REFERENCES

[1] Water distribution/<https://www.dw.com/en/are-we-running-out-of-fresh-water/a-40241057/>

[2] Water borne diseaseshttps://argucom.org.in/livpure-vs-kent-water-purifiers/

[3] Synergy enviro engineers/<http://www.synergyenviron.com/tools/solar-irradiance/india/>.

[4] Desalination and water purification technology, Bhabha Atomic research center</ http://barc.gov.in/publications/eb/desalination.pdf>/

[5] Thole B (2013) Groundwater contamination with fluoride and potential fluoride removal technologies for east and southern Africa

[6] Q. Chen, M. Kum Ja, Y. Li, K. J. Chua (2017) evaluation of solar-powered spray-assisted low-temperature desalination technology. Applied energy 211:997-1008

[7] Tan CH, Lefebvre O, Zhang J, Ng HY, Ong SL (2012) Membrane processes for Desalination: Overview.

[8] Setoodeh N, Rahimi R, Ameri A (2011) Modelling and determination of heat transfer coefficient in-basin solar still. Desalination, 268,103-110.

[9] Khare V R, Singh P A, Kumar H, Khatri R (2017) modeling and performance enhancement of single slope solar still using computational fluid dynamics. Energy Procedia,109, 447—455.

[10] Panchal H.N, Shah P K (2011) Modelling and verification of single slope still using ANSYS-CFX. International Journal of Energy and Environment,2(6), 985-998.

[11] Maheswari C.U, Reddy B.V, Sree A.N, Reddy V, Reddy S.P, Prasad R.R, Varma B.H.K (2016) Computational fluid dynamics analysis of single basin double slope solar still. Invention Journal of Research Technology in Engineering & Management, 2, 01-05.

[12] Fathy M, Hassan H, Ahmed MS (2018) Experimental study on the effect of coupling parabolic trough collector with double slope still on its performance. Sol Energy,163, 54-61.

[13] Madhlopa A, Johnstone CM (2011) computation of solar radiation distribution in a solar still with internal and external reflectors. Sol Energy, 85(2), 217-233.

[14] Panchal HN (2010) experimental analysis of different absorber plates on the performance of double slope solar still. Int J of Engineering Science and Technology, 2(11), 6626-6629.

[15] Tripathi R, Tiwari GN (2005) effect of water depth on internal heat and mass transfer for active solar distillation. Desalination, 173, 187-200.

[16] Badran O.O (2007) experimental study of the enhancement parameters on a single slope solar still productivity. Desalination, 209, 136-143.

[17] Singh N (2013) performance analysis of single slope solar stills at different inclination angles: an indoor simulation. Int J Curr Eng Technol, 3(2), 2277- 4106.

[18] Akash BA, Mohsen MS, Osta O, Elayan Y (1998) experimental Evaluation of single basin solar still using different absorbing materials. Renewable energy, 14, 307-310.

[19] Gokilavani NS, Prabhakaran D, Kannadasan T (2014) Experimental studies and CFD modeling on solar distillation system. Int J Innov Res Sci Eng Technol, 3(9), 15818-15822.

[20] Singh A, Mittal M.K. (2014) Simulation of single slope solar still at different inclinations using CFD. Int Conf Adv Res Inno,512-519.

[21] Bhaisare A, Hiwakar A, Sakhare A, Ukey S, Purty S, Wasnik U, P V.K (2019) Brackish Water Distillation System for Gorewada Water Treatment Plant, Nagpur By Using Solar Energy- A Case Study. World Journal of Engineering Research and Technology,198-215.

[22] Badusha R, Arjunan T.V (2013) Performance analysis of single slope solar still. international journal of mechanical engineering and robotics research,3(3), 2278-0149.

[23] Thakur AK, Pathak S.K (2017) Single basin solar still with varying depth of water: optimization by the computational method. Iranian Journal of Energy & Environment, 8(3), 216-223.

[24] Chinnathambi S, Sridharan M (2014) Performance enhancement study on single basin double slope solar still using flat plate collector. Int J Innov Res Eng Technol, 3(3), 1303-1308.

[25] Panchal HN, Patel N (2017) ANSYS CFD and experimental comparison of various parameters of a solar still. Int J Ambient Energy,1-7.

[26] SampathKumar K, Senthilkumar P (2012) utilization of solar water heater in single basin slope still- an experimental study. Desalination, 297, 8-19.

[27] Tabrizi FF, Sharak AZ (2010) experimental study of integrated basin solar still with a sandy reservoir. Desalination, 253, 195-199.

[28] Dimri V, Sarkar B, Singh U, Tiwari GN (2008) effect of condensing cover material on the yield of active solar still: an experimental validation. Desalination, 227, 178-189.

[29] Sharma M, Tiwari AK, Mishra DB (2016) a review on the desalination of water using single slope passive solar still. Int J Develop Research, 11, 10002-10012.

[30] Chaibi MT (2000) analysis by simulation of a solar still integrated with a greenhouse roof. Desalination, 128, 123-138.

[31] Ghoneyem A, Ileri A (1997) software to analyze solar stills and an experimental study on the effects of the cover. Desalination, 114, 37-44.

[32] Mahendren R, Senthilkumar R, Irfan Ali MD (2011) modeling of solar still using granular activated carbon in Matlab. Bonfring Int J Power Sys and Int circuits, 1, 5-10.

[33] Panchal HN, Doshi M, Chavda P, Goswami R (2011) effect of cow dung cakes inside basin on heat transfer coefficients and productivity of single basin single slope solar still. Int J App Eng Res Dindigul, 1(4), 675-690.

[34] Shukla M, Ashkedhar RD, Modak JP (2014) an experimental investigation into the performance of GI basin passive solar still using horizontal mesh and vertical mesh. Int J Res in Eng and Technol, 3, 39-63.

[35] Nayak AK, Dev R (2016) thermal modeling and performance study by modified double slope solar still. Int J Res in Eng and Technol, 5, 19-23.

[36] Abdallah S, Badran O, Abu- Khadar MM (2008) performance evaluation of the modified design of single slope solar still. Desalination, 219(1-3), 222-230.